MINERALOGICAL AND GEOCHEMICAL STUDY OF ACIDIC VOLCANIC GLASSES WITH PETROLOGICAL AND VOLCANOLOGICAL INTERPRETATION

Contributors: **Éva Balázs, Erik Dobos, Péter Rózsa, József Simulák, Sándor Szakáll**

Final Report

Compiled and edited by **Péter Rózsa**

Debrecen
2009

To the memory of Professor Gyula Szöőr (1940-2007)

who was the leader of this project until his death

Preface

Five years of study on acidic volcanic glasses are summarised in this paper. The contributors do not intend to review the research work chronologically; the report is divided into four parts.

First, study on obsidian glasses is presented. In this part, results concerning by particle induced gamma-ray emission (PIGE), laser ablation-inductively coupled plasma-mass spectrometry (LA-ICP-MS) and proton induced X-ray emission (micro-PIXE) analysis of obsidian samples from different localities of various geological settings (Armenia, Hungary, Iceland, Mexico, Slovakia, Turkey) are presented. Usability of geochemical data of obsidians for discrimination between different tectonic environments and for tracing ancient source region is also shown.

In the second part, thermoanalytical studies of weathering of acidic volcanic glassy materials are summarised. Comparing the results of X-ray diffraction, LA-ICP-OES, and thermal analysis of rhyolite tuff samples, it is demonstrated that thermogravimetry (TG) may represent a useful tool for determining weathering degree.

In the third part, a new analytical equipment, a high temperature direct probe for mass spectrometry is introduced. By using this device, small amount of gases evolved during heating can be analysed by a coupled quadrupole mass spectrometer (QMS). Although the probe has been tested by measuring gas release by silicate minerals, it may be especially useful for study of volcanic glasses.

In the fourth part, a short summary of the results is presented. Finally, it should be emphasised that several other research work concerning acidic volcanic glasses was performed in the research period, which are not discussed in this report. Some were discontinued because of fatal illness and tragic death of Professor Gyula Szöőr; others are in progress.

Péter Rózsa

1. COMPARATIVE GEOCHEMICAL STUDIES OF OBSIDIAN SAMPLES FROM VARIOUS LOCALITIES

Analysis of obsidians is great interest to archaeometry because their chemical composition can help archaeologists to find different resource areas of obsidian artefacts and to trace the possible ancient exchange centres and trade routes (see for example Bíró, 1984; Williams-Thorpe et al., 1984; Williams-Thorpe, 1995; Gratuze, 1999; Bíró, 2004). From the geological point of view, the importance of elemental constituents of obsidians is that mineralogical information can hardly be obtained on volcanic glasses. On the other hand, however, analysis of phenocrysts, which can rarely occur in volcanic glasses, may be particularly important and informative. Moreover, information on the resource area of the obsidian artefacts can be also obtained by identifying microphenocrysts present in the specimens (Kayani and McDonnell, 1996; Acquafredda and Paglionico, 2004). Our study has basically focused on the well-known obsidian occurrences in the Tokaj Mountains. On the other hand, however, obsidian samples coming from some other localities were also analysed to trace the possible geochemical differences attributed to the different geological and/or geographical settings (Table 1).

The non-destructive ion beam analysis (IBA) is suitable in general to determine major, minor and trace element content; therefore, IBA methods are widely used in geoscience research (Ryan, 2004), particularly in obsidian provenance studies (Elekes et al, 2000; Rózsa et al., 2000; Constantinescu et al. 2002; Bugoi et al. 2004). The improvement of a CLOVER-Ge-BGO detector system applied at the nuclear microprobe facility of ATOMKI (Rajta et al., 1996; Elekes et al, 1999) yielded lower detection limits on various samples in particle induced gamma-ray emission (PIGE) experiments. Moreover, application of nuclear microprobe (NMP) with use of well-established proton induced X-ray emission (PIXE) method has become more and more accepted during the last decade (Rózsa et al. 2003; Ryan, 2004; Csámer et al. 2006). NMPs have approximately similar resolution as electron microprobe (EMP) but it provides superior detection limits that are especially advantageous for measurement of minor and trace elements. Additionally, laser ablation–inductively coupled plasma–mass spectrometry (LA–ICP–MS) technique was also used.

Table 1

Locality, geological setting and age of the analysed obsidian samples

Nr	Locality	Geological setting	Geological age
1	Tolcsva, Tér Hill, Tokaj Mts., Hungary	Volcanic arc	Miocene
2	Tolcsva, Tokaj Mts., Hungary	Volcanic arc	Miocene
3	Tolcsva, Ciróka Ditch, Tokaj Mts., Hungary	Volcanic arc	Miocene
4	Erdőbénye, Tokaj Mts., Hungary	Volcanic arc	Miocene
5	Sima, Tokaj Mts., Hungary	Volcanic arc	Miocene
6	Mád, Tokaj Mts., Hungary	Volcanic arc	Miocene
7	Tokaj-Lebuj, Tokaj Mts., Hungary	Volcanic arc	Miocene
8	Vinicky, Tokaj Mts., Slovakia	Volcanic arc	Miocene
9	Lipari Islands, Italy	Volcanic arc	Quaternary
10	Kömörcü közü, Turkey	Continental collision zone	Pliocene
11	Karacaören, Turkey	Continental collision zone	Pliocene
12	Jerevan, Armenia	Volcanic arc	Pliocene–Quaternary
13	Aragats Mts., Armenia	Volcanic arc	Pliocene–Quaternary
14	Teotihuacan, Mexico	Volcanic arc	Pleistocene
15	Hrafutinussker, Iceland	Mid-ocean ridge	Holocene

The PIGE-PIXE measurements were carried out by using a scanning nuclear microprobe unit with focused proton beam (Rajta et al, 1996) installed on the 5 MV Van de Graaff accelerator of the ATOMKI, Hungary. Particle induced gamma-ray emission (PIGE) method was used for the determination of bulk composition of the samples. The proton energy, the collected charge, the beam current, the beam spot size and the scanned area were 3.3 MeV, 3 μC, 1 nA, 10 μm x 10 μm and 500 μm x 500 μm, respectively. The gamma-rays were detected by a CLOVER-Ge-BGO detector system (Elekes et al, 1999) containing four separate coaxial n-type HPGe crystals packed together in a four-leaf clover arrangement in the same cryostat. It is surrounded by a BGO shield, which acts as a veto detector. With this system extremely low detection

limits (about few ten-hundred μm/g) can be achieved for the elements in the range of 3<Z<20 (Elekes et al, 2000). The spectra were evaluated by the computer code Physics Analysis Workstation (PAW from CERN, Geneva).

Particle induced X-ray emission (PIXE) technique was used for investigation of the phenocrysts occurring in the obsidian samples. The proton energy, the collected charge, the beam current and the beam spot size were 2 MeV, 0.3 μC, 250 pA and 2 μm x 2 μm, respectively. The scanned area varied in from 20 μm x 20 μm to 1000 μm x 1000 μm. The X-rays were detected by employing two Si(Li) detectors used for detection of low (down to Na) and high energy X-rays (from Mn), respectively. For the spectrum evaluations and concentrations the program package PIXYKLM (Szabó et al, 1993) was used. The quantification of elements is based on the fundamental PIXE equations between the characteristic X-ray yields and concentrations. Self-attenuation of low energy X-rays as well as secondary (enhancement) effects are completely accounted for mathematically, and no standards are required for the concentration calculation. The testing of the reliability was also done means of obsidian standards, and it shows that even the concentration of the major elements could be determined with an accuracy of 10–15%.

The Laser-Inductively Coupled Plasma-Mass Spectrometry (LA-ICP-MS) method was used for bulk analysis of the samples, and partly for checking the concentration values determined by PIGE and PIXE techniques. The investigations were performed at the Centre de Recherches Ernest Babelon, Orléans, France. The instrument employed contains an Inductively Coupled Plasma Mass Spectrometer and a laser ablation sampling device (Gratuze, 1999). Some amount of the sample is ablated by laser beam creating pits of 40-100 μm size. The evaporated aerosol is carried to ICP and then to the quadrupole mass filter. They are collected by a channel electron multiplier assembly.

Thermoanalytical measurements for determination of water content of obsidians were carried out with Derivatograph-PC 1500 ^{o}C at the Department of Mineralogy and Geology, University of Debrecen. The series of measurement were performed under the following conditions: temperature range – 1000 ^{o}C ; rate of heating – 10 ^{o}C/minute in air (static); sample holder – platinum plate; sample weight – 1500 mg.

Major and trace elements contents of the samples obtained by LA-ICP-MS method are listed in Table 2 and Table 3, respectively. Petrographically, all samples can be regarded as rhyolites according to their position in the TAS diagram (Fig. 1). Classifying the studied obsidian samples the R1–R2 diagram (De la Roche et al, 1980), where R1 = 4Si-11(Na+K)–2(Fe+Ti) and R2 = 6Ca+2Mg+Al, was also applied. Although it is most useful and generally used for plutonic rocks, the scheme is sufficiently general to apply to volcanic rocks, too (Rollinson, 1998).

Table 2

Abundances of major elements of the obsidian samples determined by LA-ICP-MS (1-15: Table 1)

[wt%]	1	2	3	4	5	6	7	8	9	10	11	12	13	14	15
SiO_2	74,15	74,60	74,93	72,98	75,16	74,24	75,78	76,36	74,01	76,09	75,26	74,54	74,11	75,03	72,25
TiO_2	0,09	0,09	0,09	0,20	0,09	0,20	0,07	0,06	0,07	0,06	0,08	0,20	0,20	0,20	0,20
Al_2O_3	14,83	14,02	13,76	15,03	13,92	13,16	12,85	13,22	13,21	13,28	13,86	14,25	14,56	12,32	13,14
Fe_2O_3	1,39	1,29	1,39	1,79	1,39	1,78	1,20	1,19	1,59	0,90	1,10	1,20	1,10	2,29	3,18
MnO	0,04	0,04	0,04	0,04	0,04	0,03	0,02	0,04	0,06	0,06	0,05	0,07	0,07	0,15	0,08
MgO	0,07	0,06	0,07	0,16	0,07	0,13	0,03	0,06	0,04	0,03	0,06	0,17	0,17	0,05	0,05
CaO	1,36	1,24	1,24	1,43	0,99	1,26	0,67	0,95	0,73	0,55	0,80	0,93	1,12	0,32	0,70
Na_2O	3,58	3,68	3,46	3,58	3,58	3,76	3,38	3,48	4,17	4,29	4,19	4,58	4,39	4,97	5,47
K_2O	4,08	4,38	4,26	4,28	4,08	4,65	5,28	4,08	5,07	4,19	4,19	3,69	3,79	3,97	4,28
P_2O_5	0,05	0,07	0,04	0,05	0,04	0,04	0,08	0,04	0,05	0,05	0,05	0,05	0,06	0,04	0,06
H_2O-	0,17	0,25	0,25	0,22	0,40	0,28	0,00	0,15	0,13	0,16	0,17	0,21	0,28	0,27	0,25
H_2O+	0,00	0,13	0,33	0,06	0,12	0,35	0,56	0,29	0,79	0,22	0,11	0,01	0,04	0,16	0,02
sum	99,83	99,85	99,86	99,83	99,87	99,89	99,93	99,93	99,91	99,89	99,91	99,89	99,88	99,76	99,68

Table 3

Abundances of trace elements of the obsidian samples determined by LA-ICP-MS (1-15: Table 1)

|	*1*	*2*	*3*	*4*	*5*	*6*	*7*	*8*	*9*	*10*	*11*	*12*	*13*	*14*	*15*
Li	70	67	65	64	62	61	ND	72	ND	55	56	56	48	68	50
B	60	54	56	69	55	62	ND	42	ND	38	42	34	31	23	22
V	1,6	1,5	1,5	7,9	1,7	7,4	0,8	0,9	0,9	1,0	0,9	6,7	7,0	5,0	0,5
Cu	23,3	0,9	2,1	1,5	2,8	3,8	ND	1,0	ND	1,4	0,7	1,9	1,7	1,0	6,4
Zn	52	43	48	41	48	43	48	27	56	23	33	36	38	245	249
As	7,5	6,7	7,3	10	6,7	9,5	ND	6,1	ND	5,8	4,2	1,6	2,2	2,7	3,0
Rb	221	201	201	237	182	215	223	179	326	192	177	131	137	222	158
Sr	75	68	64	78	56	64	12	55	12	9	49	94	100	2	15
Y	34	28	27	32	25	23	26	20	31	15	17	16	18	118	121
Zr	138	135	114	179	103	137	86	52	140	61	98	139	150	1145	1357
Nb	19	16	17	15	15	13	11	11	35	26	23	42	47	125	247
Sb	0,4	0,5	1,8	0,6	0,3	0,7	ND	0,3	ND	0,8	0,5	0,2	0,2	0,3	0,4
Cs	9,9	8,8	9,2	10,4	7,6	9,2	10,0	9,6	17,0	7,5	7,1	4,6	4,7	4,1	1,4
Ba	729	638	635	649	533	522	109	407	12	135	254	346	386	11	208
La	41	39	38	39	30	35	38	24	46	20	25	26	26	39	141
Ce	80,6	72,8	72,8	86,2	65,2	71,5	69,0	49,1	94,0	38,0	43,6	47,0	51,1	99,3	278,0
Pr	9,4	8,4	7,9	9,8	6,8	7,9	7,5	6,1	8,8	3,6	4,7	4,7	5,4	11,8	32,1
Nd	34,6	29,3	29,0	35,3	25,4	24,7	27,0	19,2	30,0	11,6	13,1	16,2	16,2	42,7	122,0
Sm	7,2	6,1	5,6	7,6	5,6	5,7	5,6	3,5	6,0	2,1	2,5	2,1	3,8	11,3	26,4
Eu	0,8	0,5	0,8	0,9	0,6	0,7	0,2	0,1	0,1	0,1	0,3	0,5	0,7	1,6	2,3
Gd	11,6	7,3	7,0	10,7	6,0	6,5	4,9	4,6	5,5	2,4	3,6	2,0	5,9	14,6	35,8
Tb	1,1	0,9	0,8	1,2	0,7	0,8	0,8	0,7	0,8	0,3	0,5	0,5	0,5	2,7	4,7
Dy	7,1	5,6	5,4	6,7	4,5	4,9	4,3	3,7	5,3	2,6	3,5	3,4	3,8	19,0	28,9
Ho	1,3	0,9	0,9	1,3	1,0	1,0	0,9	1,0	1,0	0,5	0,6	0,3	0,9	4,9	4,8
Er	4,4	3,6	3,2	4,0	2,7	3,2	2,6	1,8	3,2	1,3	2,4	2,5	1,4	13,8	16,0
Tm	0,6	0,5	0,4	0,5	0,3	0,4	0,4	0,4	0,5	0,3	0,3	0,4	0,3	2,2	2,1
Yb	3,7	2,9	3,3	4,2	3,0	2,9	2,7	2,2	3,7	2,0	2,5	2,4	2,4	15,3	14,4
Lu	0,7	0,6	0,5	0,7	0,5	0,5	0,4	ND	0,4	0,3	0,3	0,2	0,4	2,3	2,1
Hf	5,3	5,4	4,2	5,6	3,4	5,0	3,4	1,4	5,2	2,2	3,6	4,2	5,6	33,7	37,9
Ta	1,9	1,3	1,3	1,4	1,5	1,2	1,0	1,7	2,0	2,3	2,4	2,9	4,1	8,0	16,2
Pb	36,4	29,4	2,8	35,8	34,2	22,0	33,0	29,3	28,0	24,6	26,0	16,6	21,3	40,3	15,6
Th	32,4	26,0	25,4	29,6	24,4	22,8	ND	16,0	ND	21,9	28,2	15,3	19,8	25,5	26,1
U	7,1	5,9	6,0	7,4	5,4	5,7	5,2	8,5	14,9	9,4	9,2	8,4	9,7	8,4	7,8
La/Yb	7,47	9,07	7,76	6,26	6,74	8,13	9,49	7,35	8,38	6,74	6,74	7,30	7,30	1,72	6,60
La/Sm	3,58	4,02	4,27	3,23	3,37	3,86	4,27	4,31	4,82	5,99	6,29	7,79	4,30	2,17	3,36
Eu/Eu*	0,27	0,23	0,39	0,30	0,31	0,35	0,11	0,07	0,05	0,13	0,30	0,73	0,45	0,38	0,23
Gd/Yb	2,53	2,03	1,71	2,05	1,61	1,81	1,46	1,69	1,20	0,97	1,16	0,67	1,98	0,77	2,01

ND – not detected
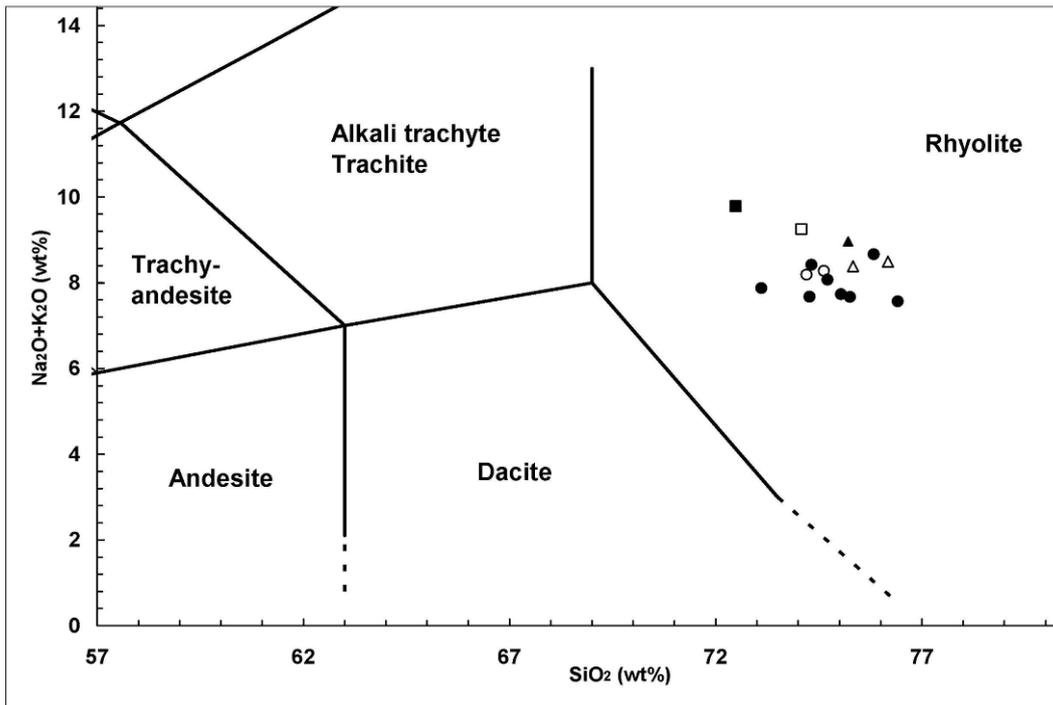
Figure 1: Position of the studied obsidian samples in the TAS diagram
Legend: full circles – Tokaj Mountains (samples 1–8); open square – Lipari Islands (sample 9); open triangles – Turkey (samples 10–11); open circles – Armenia (samples 12–13); full triangle – Mexico (sample 14); full square – Iceland (sample 15).
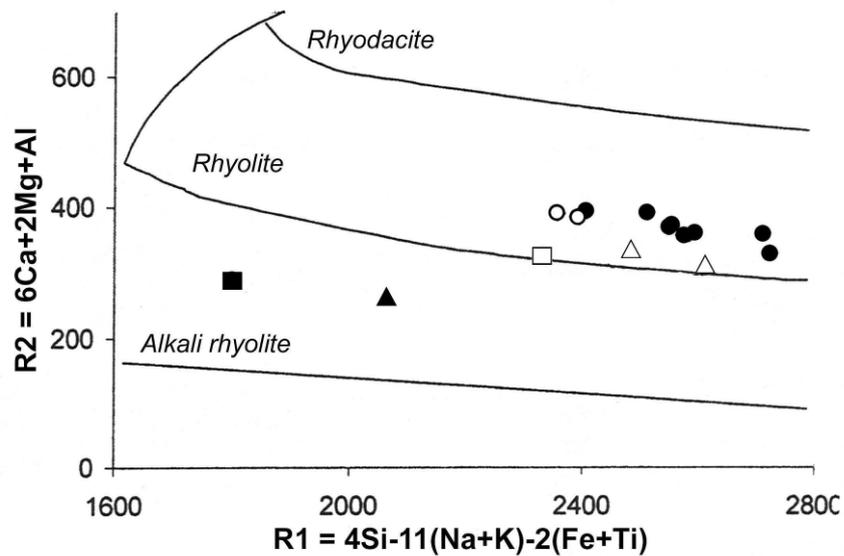

Figure 2: the Samples in the R1-R2 diagram

As Figure 2 shows samples coming from Armenia and the Tokaj Mountains belong to rhyolites; similarly, samples from the Lipari Island and Turkey also fall into this group, although their points are near the boundary line separating the rhyolite and alkali rhyolite fields. However, points of the samples coming from Iceland and Mexico are situated in the alkali rhyolite field as a consequence of their higher sodium and iron as well as lower calcium content. Obsidians are often classified chemically according to their CaO, Al_2O_3 as well as Na_2O and K_2O contents (Macdonald et al, 1993). According to this characterisation, all of the analysed samples are subalkaline–peraluminous obsidians gathering near dividing line between metaluminous and peraluminous subgroups (Fig. 3).
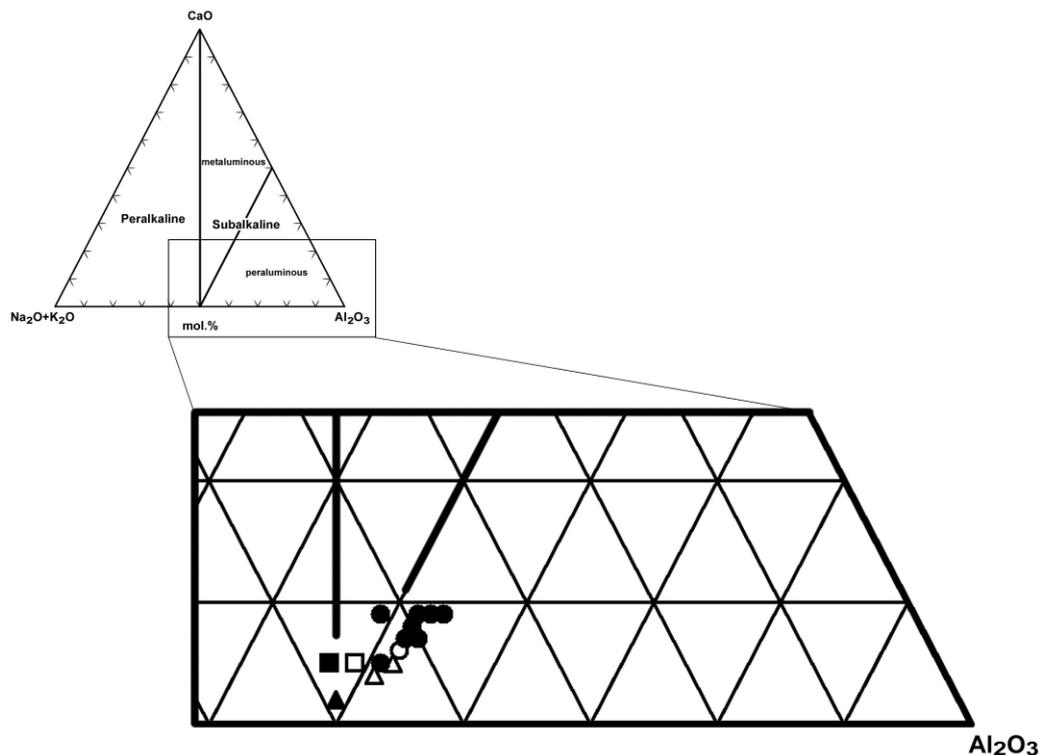
Figure 3: Samples in the CaO-Alk- Al_2O_3 triangle

Rare earth element content of the samples is listed in Table 3, and their abundances normalised to average chondrite (Boynton, 1984) are shown by Figure 4. As it can be seen, obsidian coming from Iceland has the highest concentrations for both heavy and light REE content, and, in general, samples from Turkey and Armenia contain the lowest REE concentrations. LREE pattern of obsidian sample coming from

Mexico is similar to that of samples from the Tokaj Mountains; however, its HREE content is as high as that of the sample from Iceland. La/Yb ratios range from 6.26 to 9.49, however, sample from Mexico shows an extremely low value of 1.72. The highest La/Sm ratios are characteristic for the samples from Turkey (5.99 and 6.29) and Erevan, Armenia (7.79), while the sample from Mexico has the lowest one (2.17); for the other samples, La/Sm ratios range from 3.22 to 4.82. Eu/Eu* ratios of the analysed obsidians range from 0.05 to 0.73. The highest values are represented by the Armenian samples (0.73 and 0.45), while obsidians coming from the Lipari Island and Viničky (Tokaj Mountains) have the lowest ones (0.05 and 0.07, respectively). Gd/Yb ratios range from 0,67 to 2.53. Samples coming from the Tokaj Mountains, Iceland and Aragats (Armenia) can be characterised by higher values (1.46–2.53). Obsidians from the Lipari Islands (1.20) and Karacaören, Turkey (1.16) represent lower values; moreover, samples from Kömörcü közü (Turkey), Mexico, and Erevan (Armenia) show enrichment in HREE relative to the middle REE (0.97, 0.77, and 0.67, respectively).
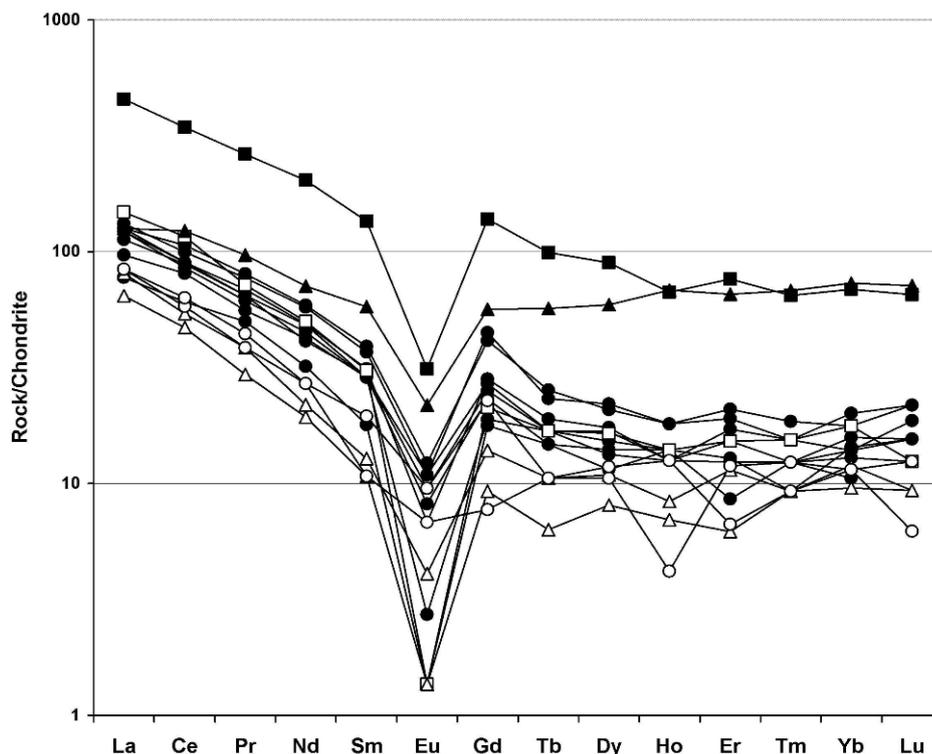
Figure 4: Chondrite-normalised REE pattern s for the studied obsidian samples. The normalising constants are from Boynton (1984).

Several variants of the spider diagrams are used for representation of trace element data, because both the order of the elements plotted and normalisation constants are varied. To maintain consistency with REE plots the trace element content of the samples is normalised to chondrite as it is proposed by Rollinson (1998). The element order and normalising values of Thompson (1982) was used with the exception of Rb, K, P, which are from primitive mantle values of Sun (1980). In this spider diagram the elements are approximately arranged in increasing compatibility from left to right. As Figure 5 shows the trace element abundance pattern of the samples is strongly spiked. Marked spikes occur at Ba, Sr, Ti and to a lesser extent Nb and P because of depletion in these elements. It is noteworthy that samples from Iceland and Mexico show Nb-Ta enrichment; however, there is a characteristic Nb-Ta trough for the other samples. Moreover, beside rare earth elements, Zr, Hf, and Y content of the samples from Iceland and Mexico is also considerable higher than that of the other samples.
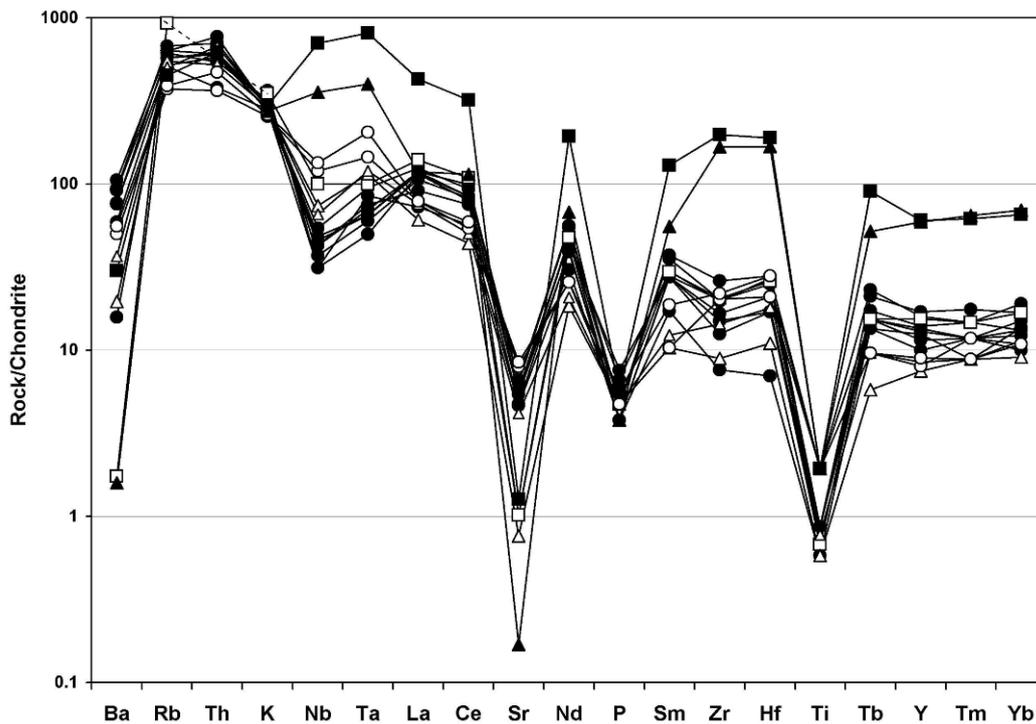
Figure 5: Chondrite-normalised trace element variation diagram for the studied obsidian samples. The normalising constants are from Thompson (1982) but Rb, K and P are from primitive mantle values of Sun (1980).

Use of discriminating diagrams to classify granites according to their tectonic setting is common in the petrologic practice (Pearce et al, 1984). These diagrams, however, can be applied for felsic lavas, too (Twist & Harmer, 1987). In the Ta–Yb and Nb–Y diagrams (Figures 6A and B, respectively) samples from Hungary dominantly belonged to the field of volcanic-arc granites (VAG) as well as that of volcanic arc and syn-collosional granites (VAG+syn-COLG) as it can be expected on the basis of their tectonic setting.

Position of samples from Turkey (syn-COLG in Figure 6A and VAG+syn-COLG in Figure 6B) also corresponds to the expectations. Armenian obsidians are described as products of a subduction related volcanic area. Their position in the Nb-Y diagram corresponds to this fact (syn-COLG in Figure 6A); however, one sample can be found in the field of within-plate granites (WPG) in the Ta-Yb diagram. The sample from Lipari Islands also belongs to the WPG fields in both diagrams.

On the other hand, however, these samples are close to the dividing line between WPG as well as syn-COLG and VAG fields. Both discrimination diagrams show the samples from Iceland and Mexico to belong to the WPG field, although they regarded as rocks associated with mid-ocean ridge and volcanic arc, respectively.

Regarding the samples coming from Iceland and Mexico their patterns in Rb–(Y+Nb) and Rb–(Yb+Ta) diagrams (Figures 6C and D, respectively) are quite similar to that of former ones, since both samples fell into the WPG field. In the Rb–(Y+Nb) diagram obsidians from Armenia and the Lipari Islands can be also found in the WPG field, although close to the boundary line between WPG and VAG as well as WPG and syn-COLG, respectively. However, all the samples coming from the Tokaj Mountains and Turkey belong to the VAG field. In the Rb–(Yb+Ta) diagram all of these samples but those of Iceland and Mexico seem to be gathered near the WPG–syn-COLG–VAG junction.
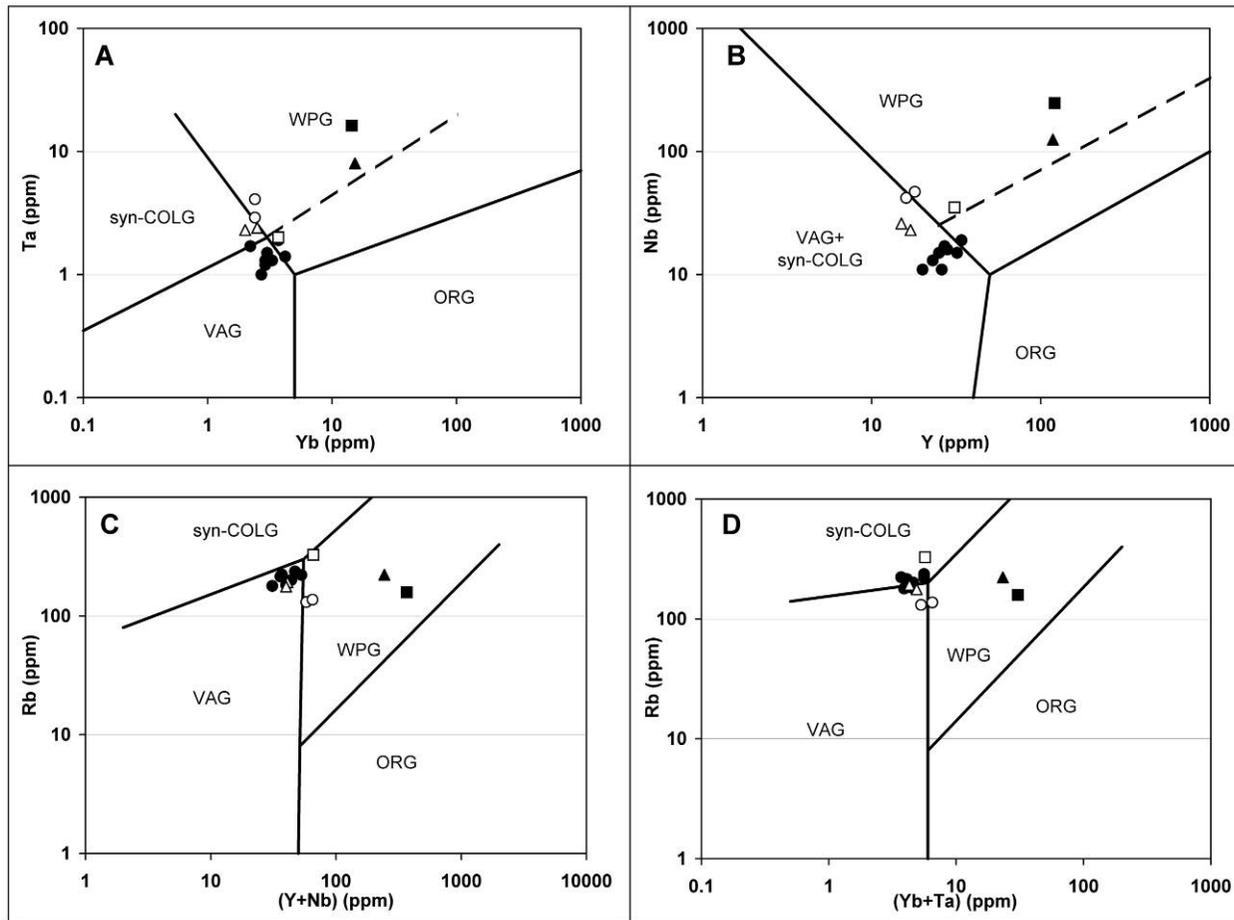
Figure 6: Distribution of the studied obsidian samples in the Ta–Yb (A), Nb–Y (B), Rb–(Y+Nb) (C) and Rb–(Yb+Ta) (D) discriminating diagrams proposed by Pearce et al (1984). (For legend see figure 1.)

Boron and lithium indicator elements are quite suitable for petrologic and petrogenetic characterisation of acid extrusive volcanic rocks (Shaw, 1996) and may provide a useful tool for tracing telethermal alteration of obsidian assemblages (Shaw and Struchio, 1992). Based on variation of the Li/B ratio of the studied samples four groups corresponding to geographic distribution (Mexico – Iceland – Turkey and Armenia – Tokaj Mountains) can be distinguished (Figure 7). It is remarkable, however, that marekanitic obsidian near Viničky, Slovakia (sample 8) differs from other samples coming from the Tokaj Mountains area (unfortunately, Li and B content of the marekanitic obsidian coming from Tokaj-Lebuj has not been measured). Using a Cs versus Ti diagram for the samples coming from the Tokaj Mountains, three groups of obsidians can be distinguished (Figure 8). Samples from Erdőbénye and Mád (sample 4 and 6, respectively) can be characterised by high Cs and Ti content; obsidians from the environment of Tolcsva (sample 1, 2, 3) and Sima (sample 5) have moderate Ti and varying Cs content; the marekanitic obsidians from Tokaj-Lebuj and Viničky (sample 7 and 8, respectively) show high Cs and low Ti concentrations.
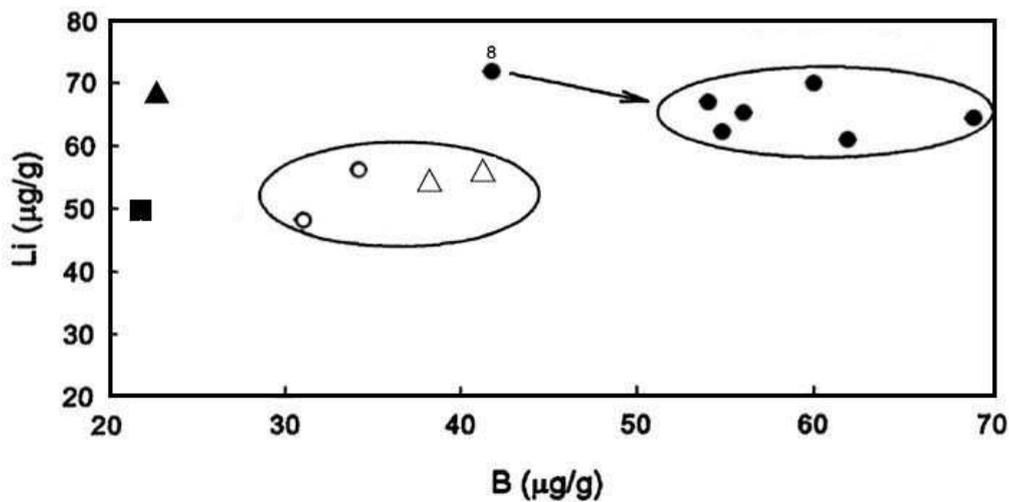
Figure 7: Distribution of the studied obsidian samples in the Li–B diagram (for legend see figure 1)
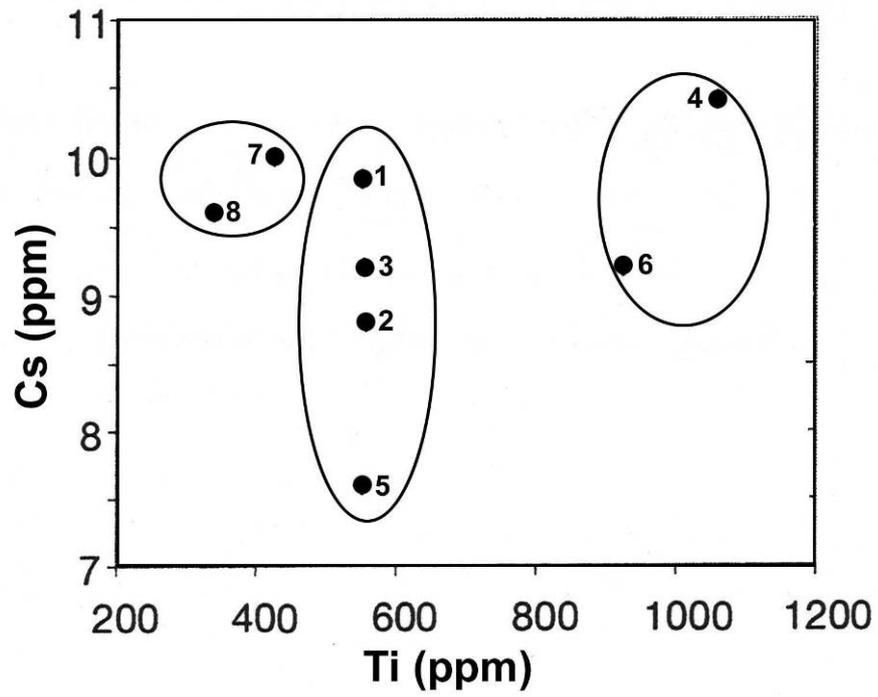
Figure 8: Distribution of the studied obsidian samples coming from the Tokaj Mountains in the Cs–Ti diagram (1–8: see table 1)

2. STUDY OF WEATHERING DEGREE OF RHYOLITE TUFF FROM EGER TOWN

Weathering process means mineralogical, petrographical and geochemical alteration of rocks, therefore characterisation of weathered state is important for determining or predicting their physical and engineering properties. In general, weathering can be regarded as an acid-base reaction where an acid is neutralised by a solid base to produce secondary minerals and dissolved salts (Helgeson et al. 1969). Essentially, weathering is a process of chemical reaction between rock (mineral) and water, as a result of which the water in the internal structure of minerals successively increases. As a consequence, a negative correlation was found between water content and different mechanical constituents (Kleb and Vásárhelyi, 2003). Moreover, different types of bonding water in soils can be used for estimating geotechnical data (Szöőr and Pittlik, 1976; Szöőr, 1978). On the basis of the well-known experience that increasing loss of ignition (LOI) may reflect increasing alteration, the simple index of chemical weathering degree (CWD) described by the following equation was proposed:

$$CWD = \frac{100(W_w - W_f)}{(W_u - W_f)} [\%],$$

where W_w is the combined water in weathered rock (%), W_f is the combined water in fresh rock (%), W_u is the combined water in the ultimate weathering product (%) (Esaki and Jiang, 1999). Some author, however, regard the 'ultimate weathering product' to be very subjective to define, and they do not recommended CWD to use (Duzgoren-Aydin et al. 2002). Although this argument can be accepted, it seems to be logic that H_2O^+ content could and should be considered an indicator of the degree of weathering. Thermal analysis makes possible to distinguish different types of bound waters in minerals (Földvári et al. 1998), therefore it could be more suitable for characterisation of weathering process than determination of LOI. In this paper comparison of analyses of rhyolite-rhyodacite tuff samples are presented. The mineralogical and major element composition of the samples was determined by X-ray diffraction and ICP-OES

techniques, respectively; quantitative measurement of different types of bound water was carried out by thermogravimetric (TG) method.

Ten samples were collected in Eger town (NE Hungary) and its near environment. Topographical positions of the sampling point were recorded by GPS, and then marked in a geological sketch map (Figure 1). The sampled formations are Miocene in age. Two samples belong to the Gyulakeszi Rhyolite Tuff Formation (Ottnangian), three of them represent the Felnémet Rhyolite Tuff Formation (Badenian-Sarmatian), one sample was collected from tuffaceous bed of the Kozárd Formation (Sarmatian), and four ones come from the Harsány Rhyolite Tuff Formation (Badenian-Lower Pannonian) (Table 1). Description of the formations can be read in the explanatory book for the 1:100000 surface geological map series of Hungary (Gyalog, 2005), and several papers have given detailed petrographic characterisation of the tuffs in the area (Szakács et al. 1998; Póka et al. 1998; Márton and Pécskay 1998)

Figure 1: Geological map of Eger town and its environment (1-10: sampling points)
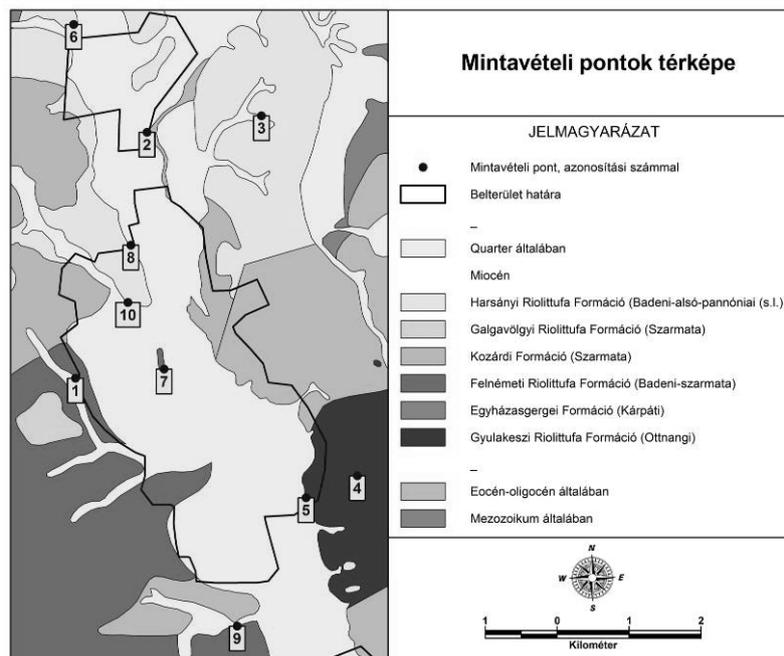
Table 1

Petrographic name, lithostratigraphic formation and locality of the samples

Nr	Petrographic name	Lithostratigraphic formation	Locality
1	rhyodacite flood-tuff	Felnémet Rhyolite Tuff F.	Eger, Szépasszony Valley
2	rhydacite tuff-tufite	Kozárd Formation	Eger-Felnémet, Szarvaskői road
3	rhyodacite flood-tuff	Harsány Rhyolite Tuff F.	Eger-Felnémet, Bajusz Field
4	pumiceous breccia	Gyulakeszi Rhyolite Tuff F.	Eger, Ostorosi road
5	rhyodacite flood-tuff	Gyulakeszi Rhyolite Tuff F.	Eger-Tihamér, Alsó quarry
6	redeposited rhyodacite tuff	Harsány Rhyolite Tuff F.	Eger-Felnémet, Csurgó Valley
7	redeposited rhyodacite tuff	Felnémet Rhyolite Tuff F.	Eger, city wall
8	rhyodacite flood-tuff	Harsány Rhyolite Tuff F.	Eger, Camping
9	rhyodacite tuff	Felnémet Rhyolite Tuff F.	Eger, Kőlyuktető
10	rhyodacite tuff	Harsány Rhyolite Tuff F.	Eger, Szala ditch

Sample preparation and density measurements were carried out in the Department of Mineralogy and Geology, University of Debrecen. Each sample was pulverized in agate mortar and dried in desiccator for two days. Density of the pulverized samples was measured by picnometer. Different types of bound waters were determined by using Mettler-Toledo TGA/SDTA 851^e thermo-microbalance equipment. 50-60 mg of the pulverized samples was analysed under static air atmosphere in the heating interval ranging from 25 to 1000 ^{o}C at a heating rate of 10 ^{o}C/min. For measurements aluminium-oxide crucibles of 150 μl were used.

To identify mineralogical composition of the samples X-ray powder diffraction was carried out in the X-ray laboratory of University of Miskolc, Department of Mineralogy and Petrology. A Bruker D8 Advance type diffractometer was used, equipped with a ceramic X-ray tube with Cu anode and long fine focus. For the measurements fixed slit system and a dynamic scintillation detector was applied with secondary graphite monochromator. The X-ray beam was produced by 40 kV accelerating voltage and 40mA tube current. Identification of the phases was implemented by Search/Match option of EVA 11, Release 2005 software.

Semiquantitative analysis of the identified phases was performed by full pattern matching procedure of the Diffrac plus Basic Evaluation Package software (EVA 11, Release 2005) without standards. Global fitting of the measured scan with another one, simulated from the PDF patterns, was applied using an empirical model for the peak shape. The method used the I/Icor coefficients from the PDF data file. It was assumed that the sum of all concentration was equal to 100%. Fitting of the scans were performed by pseudo-Voight functions as a function of 2θ. For each PDF pattern, a scan was simulated, using the positions and peak heights from the patterns and the width and shape factors of the default model provided by the EVA software. A scaling factor and the width factors were then adjusted for each pattern, in order to minimize the discrepancy between the sum of the simulated and the measured scan. X-ray amorphous components of the samples were determined by limiting the backgrounds of the scans by Bézier curves (Hubbard et al. 1976).

The major components of the samples were analysed in the Laboratory of the Geological Institute of Hungary by using a Jobin Yvon ULTIMA 2C combined (simultaneous-sequential) ICP-OES instrument. First, 0.5 g of each rock samples was weighed into platinum crucibles, then 1.16 g of $LiBO_2$ was added and mixed thoroughly. Crucibles were covered with platinum lids and were placed into electric furnace. Temperature was gradually increased up to 1060 °C. Reaching final temperature, samples were fused for 30 minutes. Crucibles were allowed to cool and then transferred into 100 mL glass beakers, covered with sufficient amount (about 50 mL) of deionised water and 10 mL of 1:1 HCl. The fusion melt was dissolved on a magnetic stirrer plate. After complete dissolution solution was transferred into volumetric flask and made up to 250 mL. (Total dissolved solid content is 2.0 g/L^{-1}). Ten times dilution of this stock solution (0.2 gL^{-1}) was used for the major component determination. The ICP-OES instrument operating parameters are the next: RF power – 1000 W; reflected power – <10 W; plasma gas flow rate – 12 L/min; sheath gas flow rate – 0.2 L/min; nebuliser type – cross-flow; nebuliser flow rate – 0.4 L/min; nebuliser pressure – 2.7 bar; observation height – 15 mm (above load coil); integration time – 0.5 s (poly) to 5 s (mono). For purging the monochromator for the determination of the UV lines nitrogene generator was applied. The -H_2O and +H_2O content were determined by gravimetric method, the FeO content was analysed by redoxy titration with $KMnO_4$

solution followed by decomposition with a mixture of H_2SO_4 and H_2F_2 in platinum crucible.

Results of the X-ray powder diffraction analyses are summarised in Table 2. As it shows plagioclase of composition varying from albite to labradorite is the essential primary mineral constituent for most of the samples; its lowest quantity is 7% (sample 4), and the highest one is 56% (sample 8), but at least 18% for the other samples. Quartz can be found in highest quantity in the samples 2 (33%) and 6 (24 %) that exceed the amount of the plagioclase feldspar in these cases (19 and 18%, respectively). Moreover, 4% of biotite, and 2-3% of sanidine can be detected in sample 1 and 2, respectively. Amorphous material, which can be regarded as volcanic glass, represents significant constituent for each samples ranging from 21 (sample 8) to 60% (sample 1). Clay minerals (mostly dickite, montmorillonite and vermiculite, rarely nontronite and sepiolite) are the most common secondary minerals. Beside clay minerals, small quantity of gypsum, erionite-like zeolite and alunogen can be also detected. On the basis of the proportion of the secondary minerals, sample 1 can be considered as relatively unaltered one, while sample 4 represents the most weathered type; the other samples are varying but moderately altered.

Major element composition and density of the studied samples is listed in Table 3. Silica content of the samples vary in wide interval, partly due to the varying degree of alteration, however, it reflects their rather rhyodacitic than rhyolitic character. Amounts of Fe_2O_3, FeO, and CaO are low, while alkali-oxides (particularly that of potassium-oxide) contents are high. Some tenth-percentages amount of sulphur in samples 1, 2 and 4 is in connection some gypsum ($CaSO_4 \cdot 2H_2O$) and alunogen ($Al_2[SO4]_3 \cdot 18H_2O$) content detected by X-ray diffraction analyses.

Table 2
Mineralogical composition of the studied samples. (Legend: al – alunogen, bi – biotite, di – dickite, er – erionite-like zeolite, gy– gypsum, mm – montmorillonite, no – nontronite, pl – plagioclase, qz – quartz, sa – sanidine, se – sepiolite, ve – vermiculite)

Nr.	Primary minerals	Amorphous	Secondary minerals
1	**37 %** (pl – 25 %, qz – 8 %, bi)	**60 %**	**3 %** (gy)
2	**55 %** (qz – 33 %, pl – 19 %, sa)	**34 %**	**11 %** (al, di, ve, mm)
3	**48 %** (pl – 38%, qz – 10%)	**30 %**	**22 %** (di, ve, mm)
4	**10 %** (pl – 7%, qz – 3 %)	**42 %**	**48 %** (mm – 32 %, no, er, se, ve, gy)
5	**50 %** (pl – 37 %, qz – 13 %)	**38 %**	**12 %** (di)
6	**42 %** (qz – 24%, pl – 18%)	**29 %**	**29 %** (mm – 24%, di, ve)
7	**55 %** (pl – 41 %, qz – 14%)	**30 %**	**15 %** (di)
8	**67 %** (pl – 56 %, qz – 11%)	**21 %**	**12 %** (di)
9	**37 %** (pl – 30%, qz – 7%)	**52 %**	**11 %** (mm, ve)
10	**47 %** (pl – 36 %, qz – 11%)	**39 %**	**14 %** (di)

Table 3
Major element composition, CIA values and density (ρ[g/cm^3]) of the studied samples.

	1	2	3	4	5	6	7	8	9	10
SiO_2	68,3	64,1	66,2	55,9	69,3	69,6	69,1	70,2	67,1	65,8
TiO_2	0,179	0,435	0,321	0,529	0,244	0,362	0,246	0,230	0,276	0,250
Al_2O_3	13,1	13,8	14,7	15,6	13,2	12,5	14,4	14,0	13,9	13,8
Fe_2O_3	1,51	3,95	2,27	3,93	1,42	3,12	1,39	0,91	1,73	2,17
FeO	0,09	0,25	0,63	0,35	0,78	0,28	0,77	0,64	0,78	0,21
MnO	0,041	0,054	0,048	0,074	0,055	0,031	0,034	0,027	0,042	0,041
CaO	2,60	1,92	2,94	2,83	3,10	1,85	2,56	2,54	1,99	2,77
MgO	0,500	0,543	0,818	1,10	0,705	0,451	0,536	0,493	0,367	0,719
Na_2O	2,16	1,28	1,91	1,17	2,36	1,68	2,48	2,45	2,17	2,52
K_2O	4,89	2,03	3,97	1,93	3,34	2,23	4,24	3,73	3,88	3,76
-H_2O	0,96	4,36	1,96	6,50	1,20	3,14	0,81	0,96	1,81	2,36
+H_2O	4,98	6,26	4,11	9,50	4,12	4,58	3,14	3,63	5,72	5,20
SO_3	0,474	0,766	- -	0,414	- -	- -	- -	- -	- -	0,196
Σ	99,78	99,75	99,88	99,83	99,82	99,82	99,71	99,81	99,77	99,8
CIA	50,52	64,35	53,76	64,77	50,4	59,83	52,21	52,74	55,28	51,76
ρ	2,3217	2,2960	2,2641	2,1357	2,4054	2,3657	2,3862	2,3740	2,3089	2,3426

Based on major element composition, several indices of weathering degree have been proposed, however, the so called chemical index of alteration (CIA) (Nesbitt and Young, 1984) is the most widely used and the most accepted one (Rollinson 1998; Duzgoren-Aydin et al. 2002; Varga et al. 2002). This index can be calculated molar proportion of aluminium-, calcium- and alkali-oxides as it follows:

$CIA = [Al_2O_3/(Al_2O_3+CaO*+Na_2O+K_2O)]$,

where CaO* represents the CaO associated with the silicate fraction. Calculated CIA values for the studied samples are listed in Table 3. According to the CIA values, sample 4 is the most altered one, and samples 1 and 5 can be regarded to be relatively unaltered. Relationship between mineralogical composition and CIA index can be displayed on a secondary minerals versus CIA diagram (Figure 2). The figure indicates an obvious but moderate correlation between the secondary mineral content and CIA values of the samples. The extraordinary position of sample 2 is due to the some % presence of alunogen. Without this sample a strong correlation can be experienced (dotted trend line in Figure 2).

Figure 2: Secondary minerals vs CIA values for the studied samples (full square marks sample 2)
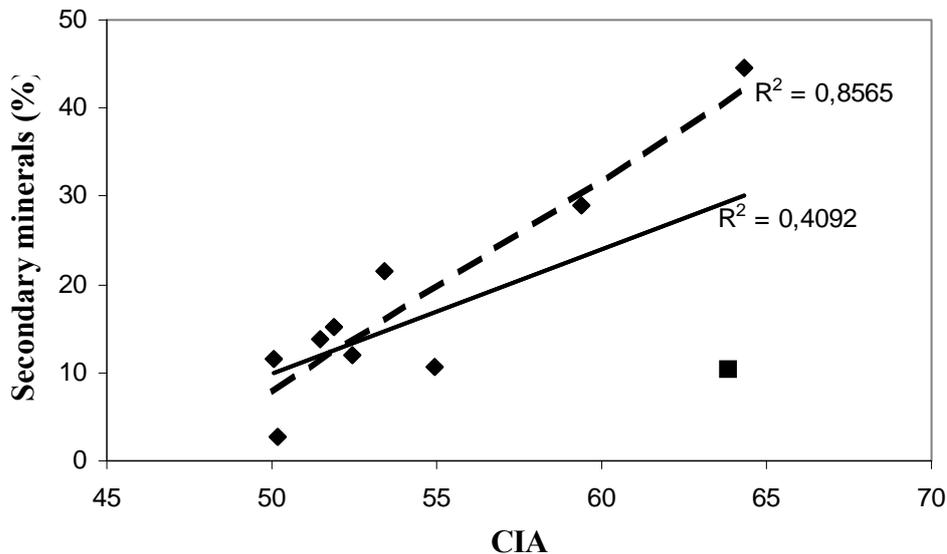
Water content of the samples is characteristically high (particularly, the $+H_2O$ values) and extremely variable indicating the advance of the alteration processes. As Figure 3 shows, there is moderate correlation of secondary mineral content to $+H_2O$, $-H_2O$ and total water content (H_2O^{total}).

Comparing water content to CIA, it must be noted that $-H_2O$ data are in relatively close correlation to CIA values (Figure 4). The measured density values are in negative connection with H_2O^{total} (Figure 5). On the basis of the linear trend of increasing density with decreasing total water content, an apparent density of 2,46 g/cm^3 can be estimated for unaltered tuff, which is in quite good agreement with other calculation (2,44 g/cm^3) (Kleb and Vásárhelyi, 2003).

Figure 3: Water content versus secondary mineral content for the studied samples
Legend: full square – $-H_2O$; open triangle - $+H_2O$; full diamond – H_2O^{total}
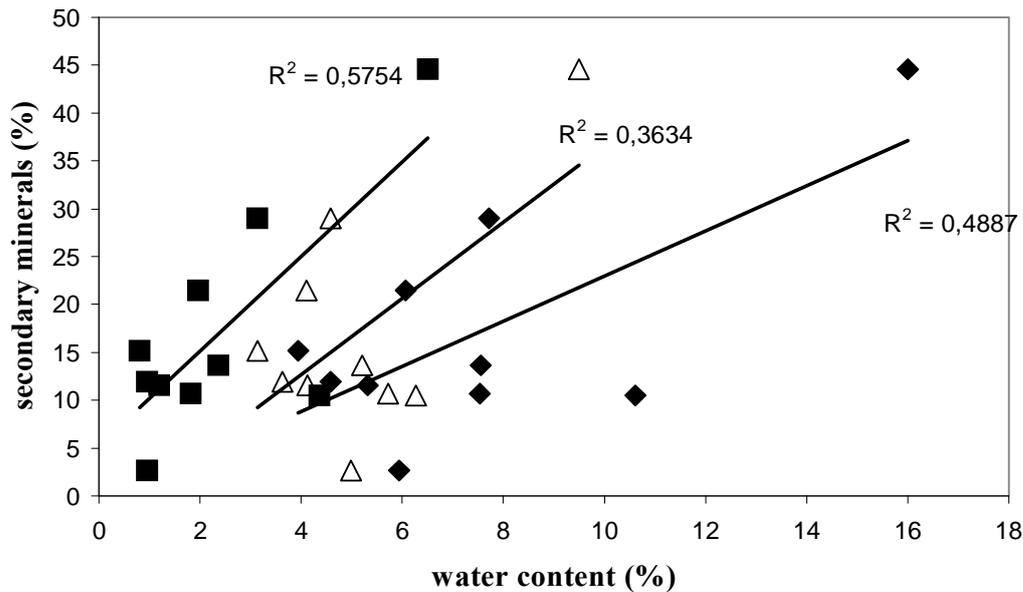
Figure 4: Correlation between water content and CIA values of the studied samples
Legend: full square – -H_2O; open triangle – +H_2O; full diamond – H_2O^{total}
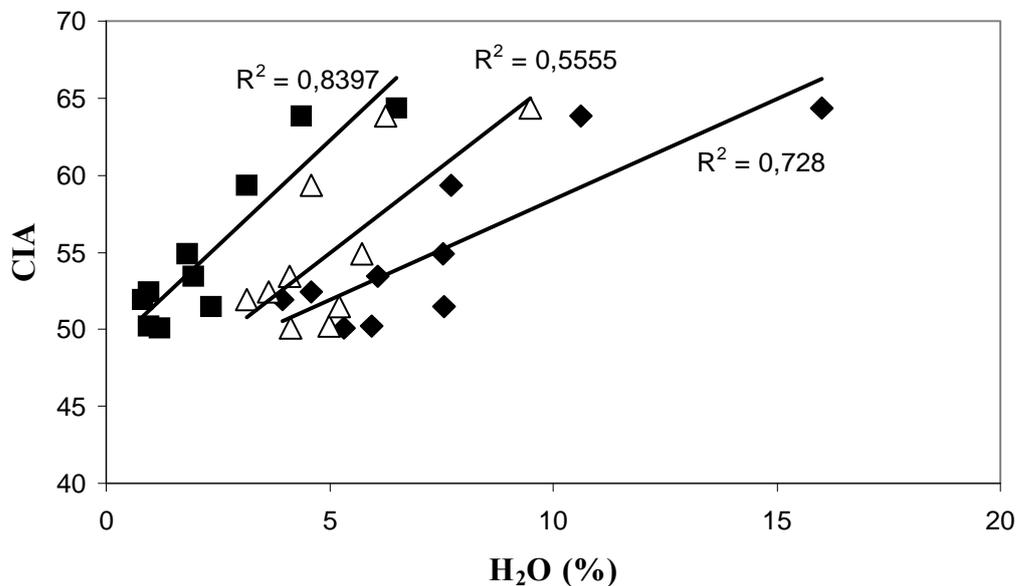
Figure 5: Correlation between density and total water content (H_2O^{total}) of the studied samples
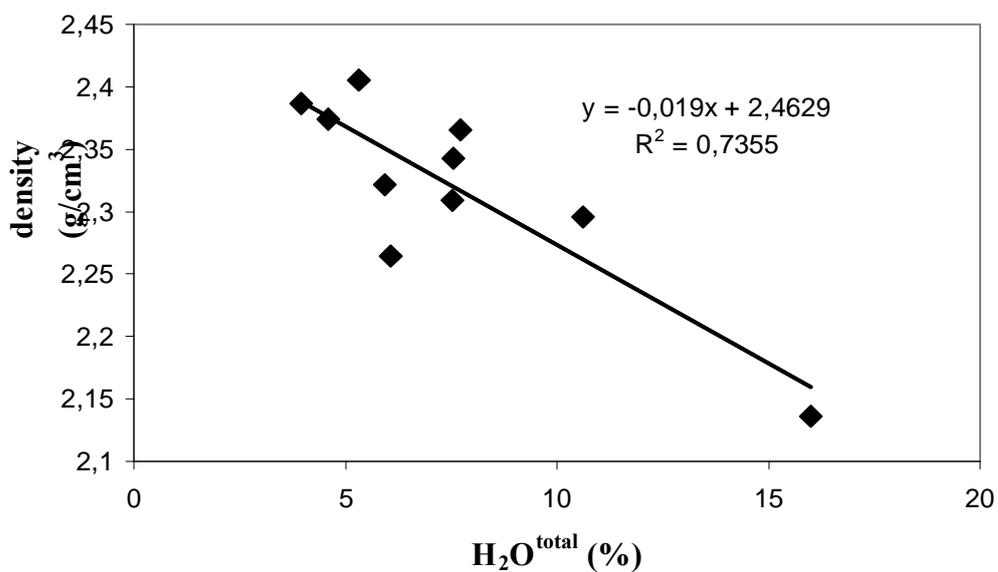
Amount of different types of bound water was measured by thermogravimetry. As Figure 6 shows, although different water types form a continuous sequence (Földvári et al. 1998), three thermal intervals and, consequently, three groups of bound water can be distinguished. Up to cca. 200 ºC adsorption water, interlayer water and some part of crystal water is released. Between cca. 200 and 500 ºC the so-called zeolitic water is lost. It is must be noted, however, that rock glasses and amorphous formations often contain water bound to zeolitic water (Földvári et al. 1998). Above 500 ºC water is released because of dehydroxylation. The above mentioned three groups of bound water are indicated as $H_2O(I)$, $H_2O(II)$ and $H_2O(III)$, respectively; the measured $H_2O(I)$, $H_2O(II)$ and $H_2O(III)$ values are listed in Table 4. Double-peak pattern of the $H_2O(I)$ regime in the case of samples 1 indicates presence of gypsum as essential secondary mineral, while the considerable water loss of sample 2 in the same regime is in connection to alunogen. The weight loss detected above 700 ºC in the cases of samples 1 and 2 is due to SO_3 release; therefore, it also indicates the presence of these sulphate minerals. In sample 4 small amount of SO_3 release also refer to gypsum, however, its double-peak in the $H_2O(I)$ regime may overlapped by absorbed water of much higher quantity coming from clay minerals.

Table 4
TG parameters (Δm [%]) of the studied samples

	1	2	3	4	5	6	7	8	9	10
$H_2O(I)$	1,12	5,23	2,25	6,80	1,79	3,69	0,95	1,24	2,18	2,29
$H_2O(II)$	3,30	1,12	2,10	4,20	2,37	1,31	2,12	2,33	3,04	2,66
$H_2O(III)$	0,53	2,88	1,40	3,27	1,11	2,16	0,87	0,66	2,00	2,00
$H_2O(I+III)$	1,65	8,11	3,65	10,07	2,90	5,85	1,82	1,90	4,18	4,29
H_2O^{total}	4,95	9,23	5,75	14,27	5,27	7,16	3,94	4,23	7,22	6,95
SO_3	0,87	1,04	- -	0,84	- -	- -	- -	- -	- -	- -

Figure 6: DTG curves of the studied samples
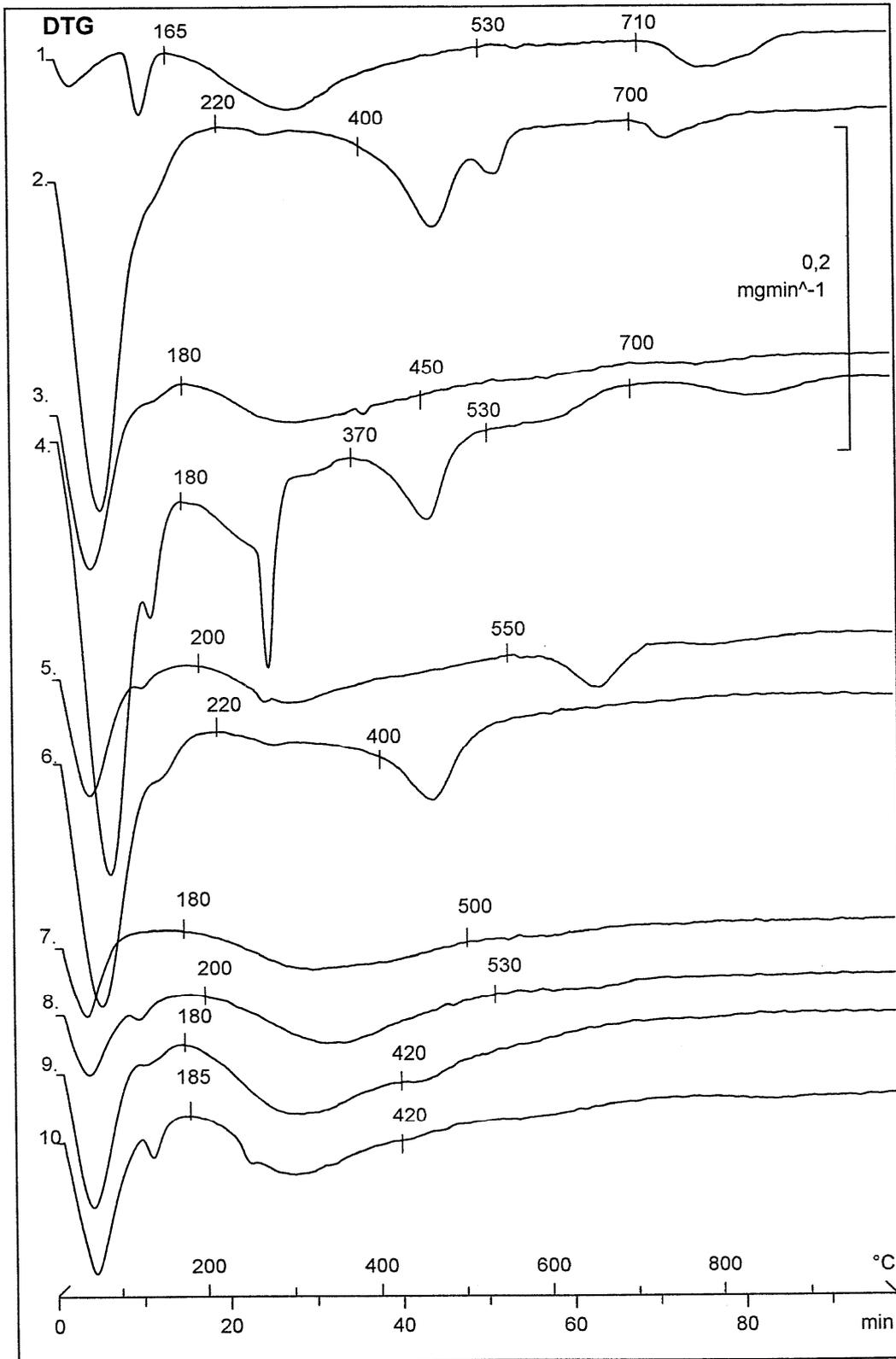
Quantity of $H_2O(II)$ shows no correlation to either secondary mineral content or CIA (Figure 7), however, as it can be assumed on the basis of previous studies (Földvári et al. 1998), it tends to increase with increasing amount of the amorphous material (Figure 8). The extreme high $H_2O(II)$ content in sample 4 indicates presence of zeolite. Without this sample, there would be a definite negative correlation of $H_2O(II)$ to both CIA and secondary mineral content.

Figure 7: $H_2O(II)$ versus CIA (squares) and secondary mineral content (triangles) for the studied samples (open square and open triangle indicate sample 4)
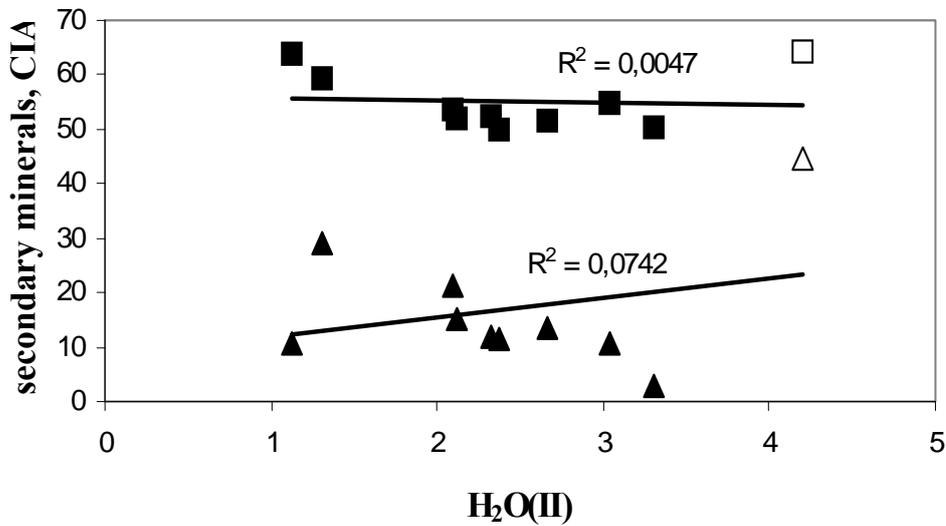
Figure 8: $H_2O(II)$ values vs amorphous material content for the studied samples
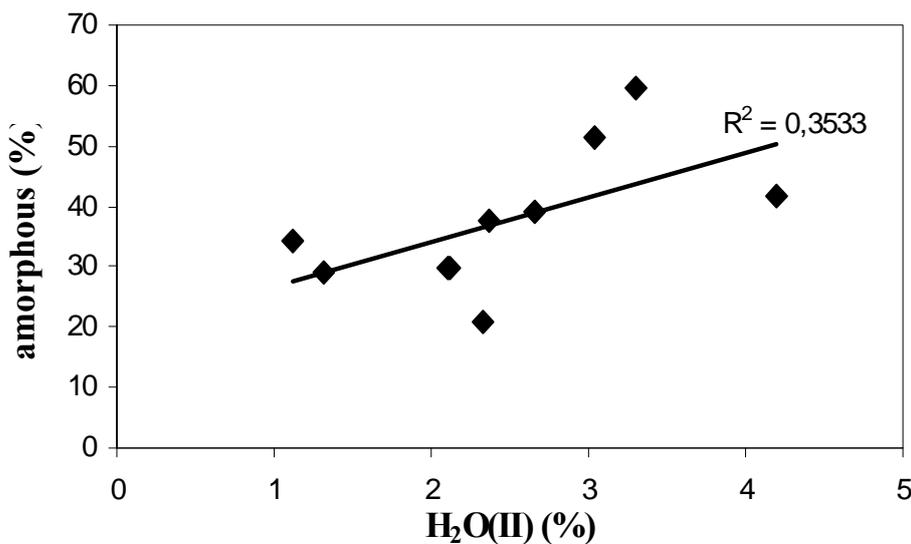
$H_2O(I)$, $H_2O(III)$ and, consequently, $H_2O(I+III)$ positively correlate to the amount of the secondary minerals (Figure 9). Similarly to the relationship between CIA and secondary minerals, the correlation is much closer if sample 2 was not taken into consideration (see dotted trend line on Figure 9).

It is also noteworthy that correlations of $H_2O(I)$ and $H_2O(III)$ to secondary mineral content are almost the same than that of CIA to secondary minerals (see Figure 1). Consequently, there is a very close positive correlation of $H_2O(I)$, $H_2O(III)$ and $H_2O(I+III)$ data to CIA values (Figure 10).

Figure 9: Correlation of different types of bound water to the secondary mineral content
Legend: full triangle – $H_2O(III)$; open square – $H_2O(I)$; full diamond – $H_2O(I+III)$
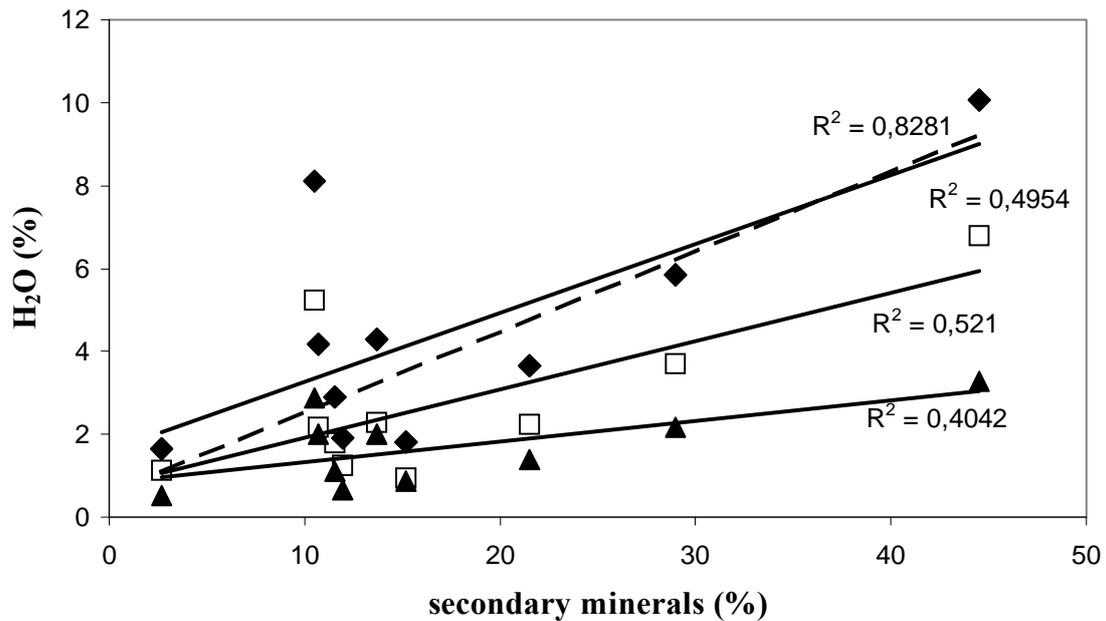
Figure 10
Correlation of different types of bound water to CIA values
Legend: full triangle – H$_2$O(III); open square – H$_2$O(I); full diamond – H$_2$O(I+III)
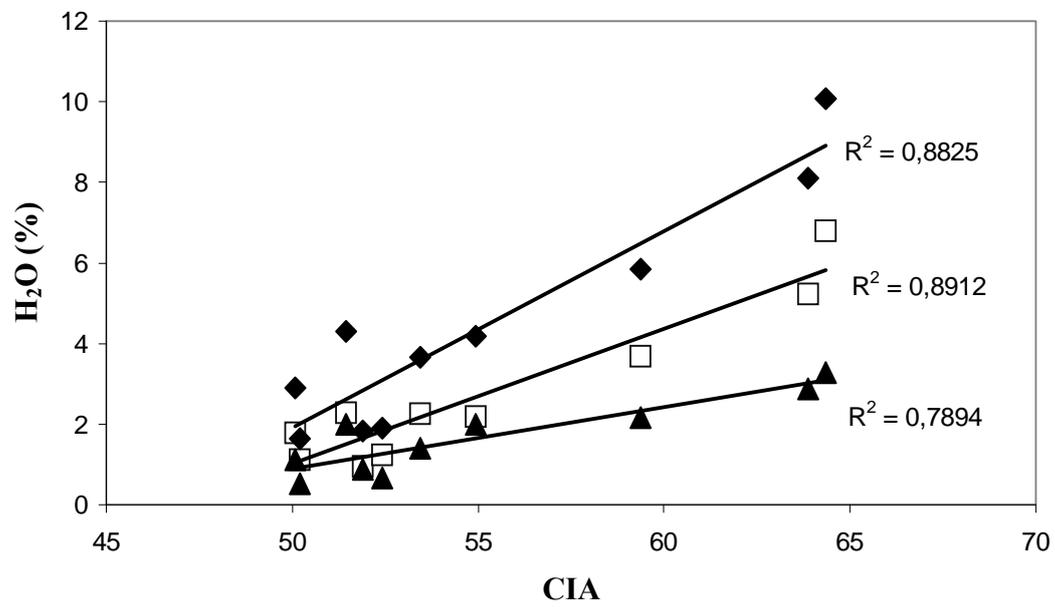
3. HIGH TEMPERATURE DIRECT PROBE FOR MS AND IT USE FOR THERMAL DECOMPOSITION MONITORING

When heating material samples ex- or endothermic thermal processes as well as weight losses may occur at temperatures characteristic of the specific components of the sample. The method is widely used in thermogravimetry (TG) and differential thermal analysis (DTA) Gaseous products of the thermal processes are determined chemically or better, by mass spectrometry (MS). Such combined instrument is frequently used to study of rocks and minerals at ambient pressure (Bohátka and Szöőr, 1987). A high temperature direct probe has been constructed for MS analysis of small amount of evolved gases (Bohátka et al. 2005).
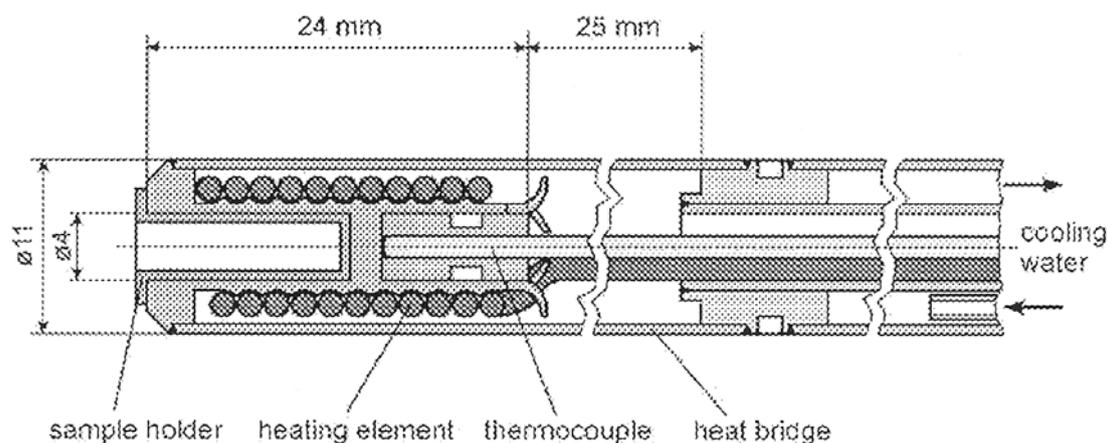
Figure 1: Schematic drawing of the high temperature direct probe

Hot parts of the probe are made of heat resistant stainless steel (H9) and Ni (Figure 1). For better contact the heating element (Thermocoax SEI 15/50 is wound on a threaded body that includes the sample holder on the upper end and a thermo-couple at the bottom. The threaded body is Ar-welded into the covering tube after assembling the parts of the probe. There is a thin-walled heat bridge (length: 25 mm) between the heater and water-cooled handle of the complete probe. The handle is sealed with a vitron O-ring and, after fore-vacuum pumping, it is gated into the MS system through a ball valve. A PID controller (Omron E5CK) controls heating. Programmable parameters are the number of steps in which the ultimate temperature is achieved, the rate of heating and the length of constant temperature periods in each step. Maximum operating temperature is 800°C.

The probe was coupled to a quadrupole mass spectrometer (QMS) (Q300C, ATOMKI) so that it is mounted next to the ion source with its axis perpendicular to that of the QMS and with a slope of 10° (to avoid dispersion of the sample). The distance from the ion source is adjustable but 5 mm was found to be optimum. Tightly fitted, replaceable quartz and stainless-steel sample holders are used. The mass range of the computer-controlled quadrupole is 1-300 a.m.u. A diffusion pump of 600 ls^{-1} and Santovac-5 oil produce a low background of $3x10^{-8}$ mbar and an order of magnitude less when cooling the oil trap with liquid nitrogen. The working chamber is kept at 100^oC. For better gas release and to avoid abrupt bursts samples are ground. After carefully pumping the sample and positioning the probe at the ion source, the radiant heat from the hot filament gradually raises its temperature, resulting in early evolution of weakly bound volatiles that overlap on desorbed gases.

The probe and the system was first tested by measuring gas release from $CaCO_3$ and $Ca(COO)_2 .H_2O$; then hyalophane feldspar and buddingtonite were studied. DTA and TG measurements of the minerals were made using a Derivatograph-PC (MOM, Hungary) in air with a dynamic heating of 10^oC s^{-1} and in a Pt crucible. Samples of 10-30 mg were analysed using the QMS. When comparing the results of TG, DTA analyses at atmospheric pressure and MS measurements in vacuum we should note that the exact temperatures resulting in gas release are different under different pressure conditions; only the trend is similar. TG and DTA curves of hyalophane feldspar show a mass loss equal to 0.08% of the original mass in an endothermic reaction at about 80^oC and 0.21% more above 200^oC (Fig. 2). From the time function of ion signals monitored with MS (Fig. 3) it is seen that the first reaction was the release of volatile NH_3 and H_2O (masses 18, 17, 16, 15 a.m.u.). In the range of 300-600°C (with a maximum at 375°C) CO_2, N_2 and again ammonia, water appear. At these higher temperatures the source of evolved ammonia is NH_4^+ bound to feldspar. The presence of CO_2 is obvious from the curves of masses 44 ad 12. The release of N_2 is more probable than CO because of the nature of the mineral and because the intensity of mass 14 increases in parallel with that of mass 28. It was proved in experiments with an empty probe that the increase of intensities of masses 28, 12 and partly 44 (CO, CO_2, hydrocarbons) above 600°C can be explained as degassing of the surfaces around the probe due to heat radiation. The transition of the

quartz causes a large change in the DTA curve at 575°C but this is not connected with gas evolution.

Figure 2: Thermoanalytical curves of a sample from hyalophane-quartz vein


Hyalophane feldspar, Quartz; Zagrlski Potok, Bosnia
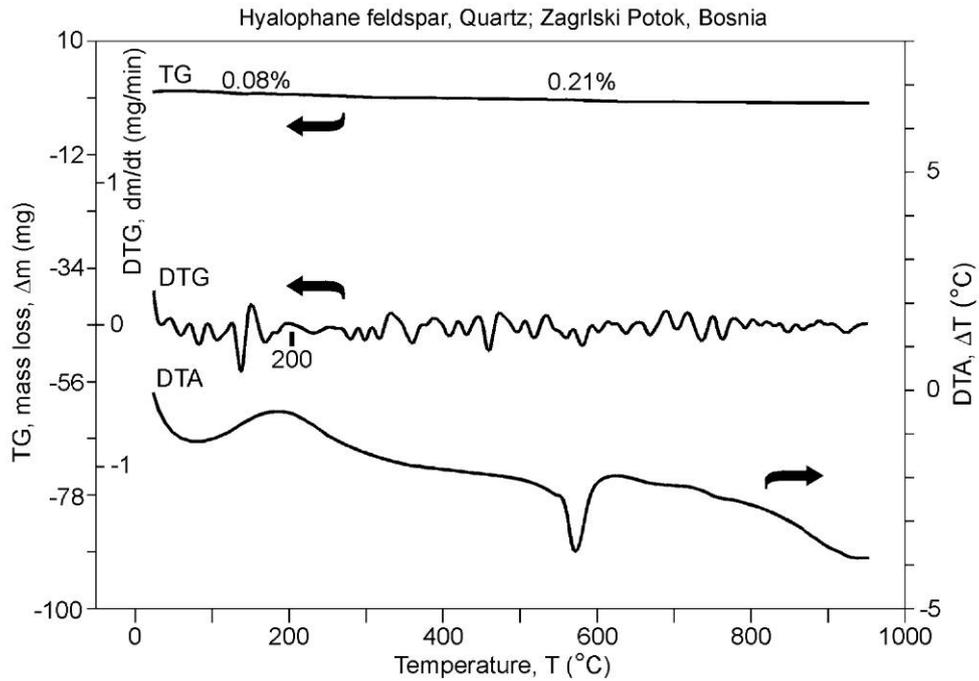
Figure 3: MS analysis of evolved gases from a hyalophane-quartz vein showing ion intensities as function of time. Figures denote the mass numbers of the monitored ions. Dashed lines refer to a tenfold magnification of the original intensity.
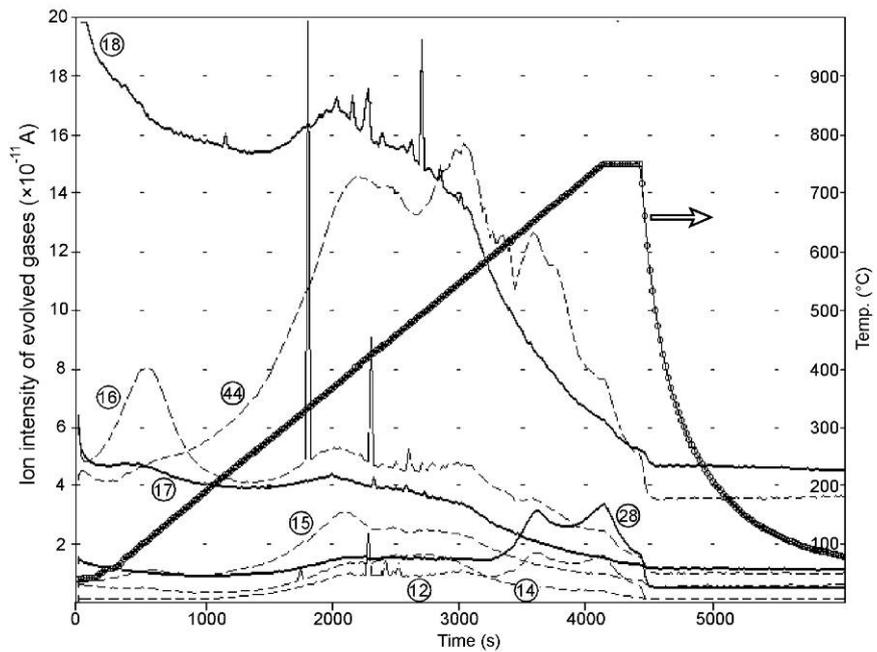
Buddingtonite samples yield more steps (Figs. 4 and 5). The first one at 30°C is due to water desorption; later volatile NH_3 gives a smaller rise in masses 15, 16, 17 at 80°C. Small quantities of NH_3 and H_2O are evolved at 205°C. Mostly water bound to buddingtonite is responsible for the large gas release between 250 and 550°C, showing a maximum at 390 and 490°C. Ammonia also contributes to this increase especially at the first peak but its signal (see masses 15, 16) gradually decreases.

The next big water peak is at 600°C. Synchronous intensities of ions of 12, 28 and 44 represent a small amount of CO_2 which is evolved from about 200°C, showing peak at 350 and 600°C. CO_2 comes from the carbonate components of the rock sample. Without tandem MS the presence of CO cannot be excluded but N_2 is most likely because of the nature of the mineral. The intensity ratio of CO^+ and CO_2^+ ions increases with temperature as the decomposition yield of CO_2 is increasing. Similar decomposition of NH_3 yielding N_2 and N is observed in good accordance with former results (Oh et al. 1993). Above 600°C ammonia evolves first in NH_3 form (this is indicated by the peaks of ions at 17 at 660 and 740°C). Ionically bound NH_4^+ is the main source around 680°C (peaks of the curves of masses 18, 28, 14) but the relatively high peaks at 14 and 28 are indications of the decomposition of NH_4^+. The high peak of mass 28 cannot represent CO because it is not accompanied by a signal of mass 12.

**Figure 4: Thermoanalytical curves of a buddingtonite sample**
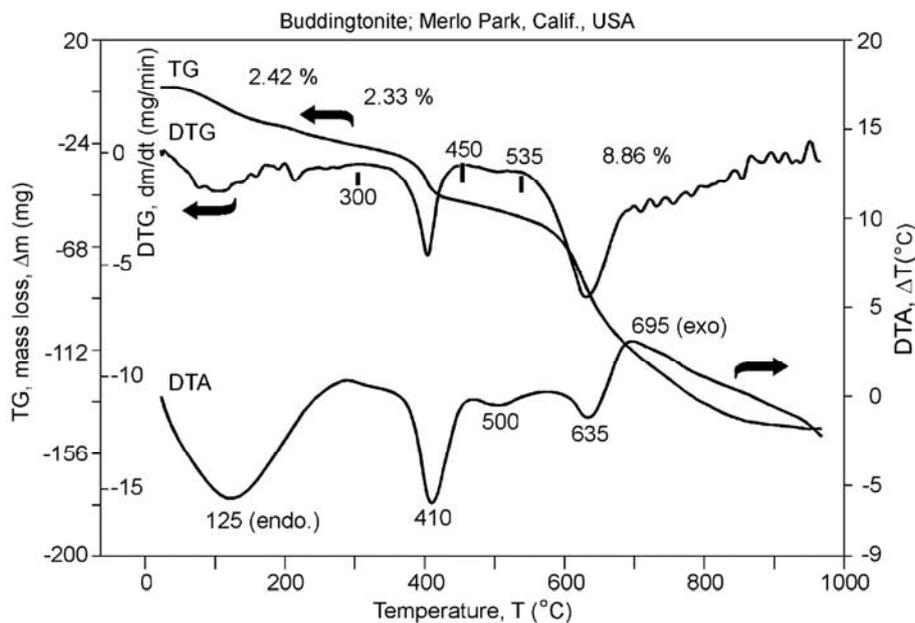
Figure 5: MS analysis of evolved gases from a buddingtonite sample showing ion intensities as a function of time. Figures denote the mass numbers of the monitores ions. Dashed lines refer to a tenfold magnification of the original intensity
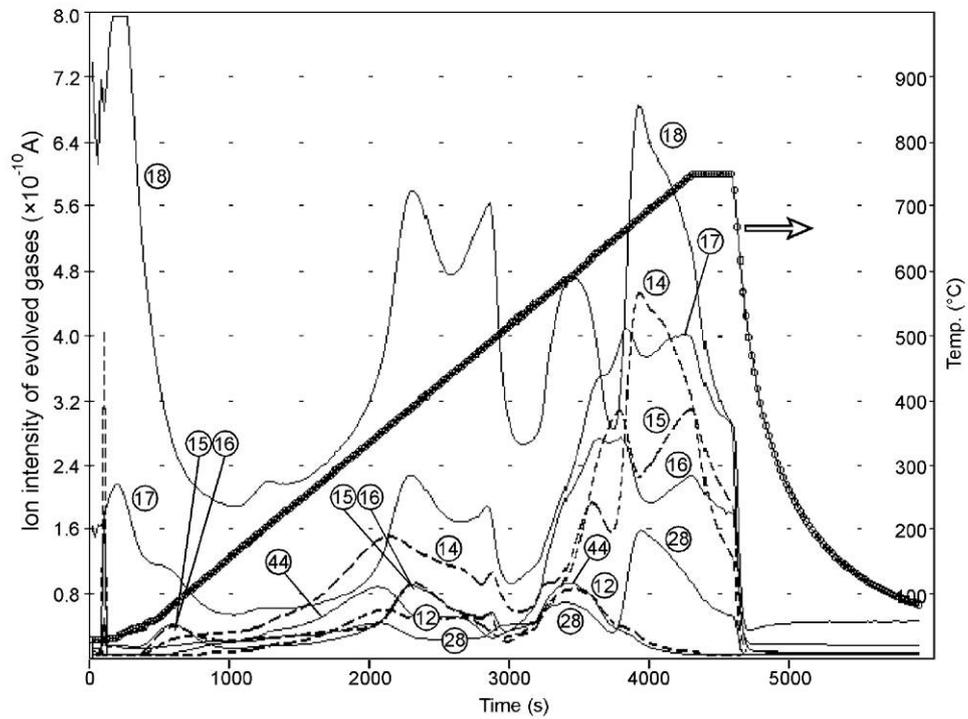
4. SUMMARY OF THE RESULTS

I)   Concerning study of obsidians from various localities, the results of the research presented in the report can be summarised as it follows:

a) According to the TAS diagram, the analysed obsidian samples can be regarded as rhyolites. Similarly, they are classified as rhyolites in the R1–R2 diagram; however, points of the samples coming from Iceland and Mexico fall into the alkali rhyolite field. Position of these two samples in the $CaO–(Na_2O+K_2O)–Al_2O_3$ triangle also indicates their relative alkali enrichment.

b) Obsidian samples from Iceland and Mexico differ from the other samples concerning their REE and trace element content, too. Sample from Iceland has the highest heavy and light REE content, and, HREE content of the obsidian from Mexico is as high as that of the sample from Iceland.

c) Trace element abundances of the samples are strongly spiked for all of them, basically, because of depletion in Ba, Sr, Ti and to a lesser extent P. Samples from Iceland and Mexico show Nb-Ta enrichment; on the other hand, however, there is a characteristic Nb-Ta trough for the other samples. This difference of the trace element patterns of obsidian samples is similar to that of alkalic oceanic-island basalts and subduction related calc-alkaline basalts, respectively (Thompson et al., 1984), although the peak is not so high, and the through is not so deep in the cases of the obsidian samples; therefore, it seems that trace element abundance patterns characteristic for basalts from different tectonic settings could be applied for acid igneous rocks, too.

d) All discrimination diagrams show the obsidian samples from Mexico and Iceland to belong to WPG field, which is in accordance with their REE and trace element patterns as well as with their alkali character indicated by the R1–R2 diagram and the $CaO–Na_2O+K_2O–Al_2O_3$ triangle, and suggests that within plate volcanism may played role in their genesis. Position of the samples from the Tokaj Mountains is definite, and, with the exception of Rb–(Yb+Ta) diagram, it corresponds to the expectation (VAG or VAG+syn-COLG fields). On the other hand, position of samples from the Lipari Islands, Turkey and Armenia in the discrimination diagrams is not consequent.

e) On the basis of lithium and boron content of obsidians coming from various localities three groups corresponding to their geographic distribution could be distinguished (Mexico and Iceland − Turkey and Armenia − Tokaj Mountains). Moreover, using a Cs versus Ti diagram for the samples coming from the Tokaj Mountains, three groups of the localities (Erdőbénye-Mád − Tolcsva-Sima − Tokaj-Viničky) can be distinguished. These categories are in good accordance with the archeometrical classification concerning the Carpathian obsidians (Williams-Thorpe et al., 1977; Bíró, 2004; Kasztovszky and Bíró, 2004): the first two groups certainly correspond to the Carpathian IIE (C2E) and Carpathian IIT (C2T) obsidian source areas, respectively, while the third one may belong to the Carpathian I (C1) group. Moreover, the presented analytical data concerning Erdőbénye, Tokaj, and the Lipari Island recently are regarded as standards (Calcagnile et al. 2007; Butalag et al. 2008; Demortier et al. 2008).

II) Regarding our studies concerning weathering of rhyolite tuffs the following relationships were found:

a) Amount of secondary minerals shows obvious but moderate positive correlation to CIA as well as $H_2O(I)$, $H_2O(III)$ and $H_2O(I+III)$ values.

b) Correlation of secondary mineral content and CIA is quite similar to that of secondary mineral content and $H_2O(I)$, $H_2O(III)$ and $H_2O(I+III)$.

c) $H_2O(II)$ shows no correlation to both secondary mineral content and CIA, however, it is positive correlation to amount of amorphous material.

d) CIA is in close positive correlation to $H_2O(I)$, $H_2O(III)$ and $H_2O(I+III)$ values. These correlations are, in general, remarkably closer than that of CIA to total water content (H_2O^{total}) or even to -H_2O.

e) Considering the above mentioned relationships, it can be concluded that validity of some TG H_2O parameters, such as $H_2O(I)$, $H_2O(III)$ and $H_2O(I+III)$ for indicating alteration of rocks is very similar to that of CIA. It would be desirable to determine more precise correlation between TG H_2O parameters and CIA, however it requires further studies on numerous samples.

f) Recently, some authors emphasised that geochemical signatures of weathering should be used to establish a framework for further interpretation and prediction

rather than quick classifications using different indices (Duzgoren-Aydin et al. 2002). By using thermogravimetric methods, not simply the different types of bound water can be determined, but essential petrographical and mineralogical conclusions can be drawn concerning the weathering process, too (Földvári et al. 1998). Consequently, thermogravimetry, and other thermal analytical methods, may serve not simply as useful tool for estimation and characterisation of weathering degree of rocks, but might be considered as an essential part of this framework.

III.   A useful probe has been constructed to introduce and heat, according to a preset program, small amounts of solid materials into a mass spectrometer. Gases evolved from the heated samples can be mass analysed in the low high vacuum range from room temperature up to 800°C. After testing the apparatus with thermoanalytical standards, minerals were studied. It was possible to measure nitrogen compounds in different mineralogical samples such as ammonium ion in K- and Ba-bearing feldspars and in the form of trapped volatile inclusions (NH_3, N_2). The quartz component of the vein proved to be free from N-compounds. The total evolved gas content of the hyalophane-quartz sample represents a mass loss of 0.29% and from that amount the quantity of ammonia is even less, but of the same order as the amount determined by Beran et al (1992).

REFERENCES

Acquafredda, P., Paglionico, A. 2004. Eur. J. Mineral. 16. 419–429.

Bartha, L., Uzonyi, I. 2000. Nucl. Inst. Meth. B. 161. 339–343.

Beran, A., Armstrong, J., Rossman, G. 1992. Eur. J. Mineral. 4. 847–850.

Bíró, K.T. 1984. Acta Archaeologica Carpathica, 23. 5–42.

Bíró, K.T. 2004. Archeometriai Műhely 2004/1. 3–8. (in Hungarian)

Bohátka, S., Szöőr, Gy. 1987. Vacuum 37. 187–188.

Bohátka, S., Szöőr, Gy., Czél, Gy., Balázs, É. 2005. Vacuum 80. 247–252.

Boynton, W.V. In: Henderson, P. (ed.): Rare earth elements geochemistry. Elsevier, 1984, 63–114.

Bugoi, R., Constantinescu, B., Neelmeijer, C., Constantin, F. 2004. Nucl. Inst. Meth. B. 226. 136–146.

Butalag, K., Calcagnile, L., Quarta, G., Maruccio, L., D'Elia, M. 2008. Nuclear Instruments and Methods in Physics Research B, 266. 2353–2357.

Calcagnile, L., Quarta, G., Butalag, K., Maruccio, L., D'Elia, M., Caramia, A., Lamura, G. In: J. Miranda, J.L. Ruvalcaba-Sil, O.G. de Lucio (eds): Proceedings of the XI International Conference on PIXE and its Analytical Applications (Puebla, Mexico, May 25-29,2007)PI-41-1–5, UNAM, Mexico City, 2007

Constantinescu, B., Bugoi, R., Sziki, G. 2002. Nucl. Inst. Meth. B. 189. 373–377.

Csámer, Á., Elekes, Z., Rózsa, P., Uzonyi, I., Kiss, Á.Z., 2006. J. Radioanal. Nucl. Chem. 268. 3. 511–516.

De la Roche, H., Leterrier, J., Grandeclaude, P., Marchal, M. 1980. Chem. Geol. 29. 183–210.

Demortier, G., Quarta, G., Butalag, K., D'Elia, M., Calcagnile, L. 2008. X-Ray Spectrometry, 37. 2. 178–183.

Duzgoren-Aydin, N.S., Aydin, A., Malpas, J. 2002. Engineering Geology 63. 99–119.

Elekes, Z., Kiss, Á. Z., Gyürky, Gy., Somorjai, E., Uzonyi, I. 1999. Nucl. Instr. Meth. B 158. 209–213.

Elekes, Z., Uzonyi, I., Gratuze, B., Rózsa, P., Kiss, Á. Z., Szöőr, Gy. 2000. Nucl. Instr. Meth. B 161/163. 836–841.

Esaki, T., Jiang, K., 1999. Engineering Geology 55. 121–130.

Földvári, M., Paulik, F., Paulik, J. 1998. J. Thermal. Anal. 33. 121–132.

Gratuze, B. 1999. J. Archaeological Science 26. 869–889.

Gyalog, L. (ed.): Explanatory to covered geological map of Hungary 1:100000, Geological Institute of Hungary, Budapest 2005 p. 189 (in Hungarian)

Helgeson, H.C., Garrels, R.M., Mackenzie, F.T., 1969. Geochim. Cosmochim. Acta 33. 455–481.

Hubbard, C.R., Evans, E.H., Suith, D.K. 1976. J. Appl. Cryst. 9. 169–174.

Kayani, P.I., McDonnell, G. 1996. Archeometry 38. 43–58.

Kasztovszky, Zs., Bíró, T.K. 2004. Archeometriai Műhely, 2004/1. 9–15. (in Hungarian)

Kleb, B., Vásárhelyi, B., 2003. Acta Geol. Hung. 46. 301–312.

Macdonald, R., Smith, R.L., Thomas, J. E.: Chemistry of the subalkalic silicic obsidians. US Geol. Survey Professional Paper. Washington, 1993.

Márton, E. Pécskay, Z. 1998. Acta Geol. Hung. 41. 467–485.

Nesbitt, H.W., Young, G.M. 1984. Geochim. Cosmochim Acta 48. 1523–1534.

Oh, M.S., Foster, K.G. Alcaraz, A., Crawford, R.W., Taylor, R.W., Coburn, T.T. 1993. Fuel 72. 517–523.

Pearce, J. A., Harris, N. B. W., Tindle, A. G. 1984. J. Petrology 25. 956–983.

Póka, T., Zelenka, T., Szakács, A., Seghedi, I., Nagy, G., Simonovits, A. 1998. Acta Geol. Hung. 41. 437–466.

Rajta, I., Borbély-Kiss, I., Mórik, Gy., Bartha, L., Koltay, E., Kiss, Á. Z. 1996. Nucl. Instr. Meth. B 109/110. 148–153.

Rollinson, H.: Using geochemical data. Longman, 1998. p. 352.

Rózsa, P., Szöőr, Gy., Simulák, J., Elekes, Z., Beszeda, I. In: Rammlmair, D. et al (eds): Applied Mineralogy I. Balkema, Rotterdam, 2000. 217–220.

Rózsa, P., Elekes, Z., Szöőr, Gy., Simon, A., Simulák, J., Uzonyi, I., Kiss, Á.Z. 2003. J. Radioanal. Nucl. Chem. 256. 329–337.

Ryan, C. G. 2004. Nucl. Instr. Meth. B 219/220. 534–549.

Shaw, D. M. In: Grew, E. S., Anovitz, L. M. (eds.): Boron: Mineralogy, petrology and geochemistry. Review in Mineralogy 33. 745–769. Geological Society of America, 1966. p. 862.

Shaw, D. M., Sturchio, N. C. 1992. Geochim. Cosmochim. Acta 56. 3723–3731.

Sun, S.S. 1980. Phil. Trans. R. Soc. Lond. A297, 409–445.

Szabó, Gy., Borbély-Kiss, I. 1993. Nucl. Instr. Meth. B 75. 123–126.

Szakács, A., Seghedi, I., Zelenka, T., Márton, E., Pécskay, Z., Póka, T.1998. Acta Geol. Hung. 41. 401–412.

Szöőr, Gy. 1978. Bull. Hung. Geol. Soc. 108. 577–581. (in Hungarian)

Szöőr, Gy., Pittlik, E. in Á. Kézdi and I. Lazányi (eds.), Proceedings of the fifth Budapest Conference on soil mechanics and foundation engineering, Akadémiai Kiadó, Budapest 1976 pp. 201–210.

Szöőr, Gy., Elekes, Z., Rózsa, P., Uzonyi, I., Simulák, J., Kiss, Á.Z. 2001. Nucl. Instr. Meth. B 181. 557–562.

Thompson, R.N. 1982. Scott. J. Geol. 18. 49–107.

Thompson, R.N., Morrison, M.A., Hendry, G.L., Parry, S.J. 1984. Phil. Trans. R. Soc. Lond. A310, 549–590.

Twist, D., Harmer, R.E.J. 1987. J. Volc. Geothermal. Res. 32. 83–98

Uzonyi, I., Rajta, I., Bartha, L., Kiss, Á. Z., Nagy, A. 2001. Nucl. Instr. Meth. B 181. 193–198.

Varga, A., Szakmány, Gy., Raucsik, B., Hartyáni, Zs., Szilágyi, V., Horváth, T. 2002. Hungarian Journal of Chemistry, 108. 387-396. (in Hungarian)

Williams-Thorpe, O. 1995. Archaeometry. 37. 217–248.

Williams-Thorpe, O., Warren, S.E., Nandris, J. 1984. J. Archaeological Science, 11. 183–212.